



# Alleviating inhibitory effect of H<sub>2</sub> on low-temperature water-gas shift reaction activity of Pt/CeO<sub>2</sub> catalyst by forming CeO<sub>2</sub> nano-patches on Pt nano-particles

Jaeha Lee<sup>a</sup>, Dongjae Shin<sup>b</sup>, Eunwon Lee<sup>a</sup>, Chengbin Li<sup>c</sup>, Ji Man Kim<sup>d</sup>, Jeong Woo Han<sup>b</sup>, Do Heui Kim<sup>a,\*</sup>

<sup>a</sup> School of Chemical and Biological Engineering, Institute of Chemical Processes, Seoul National University, Seoul 08826, Republic of Korea

<sup>b</sup> Department of Chemical Engineering, Pohang University of Science and Technology (POSTECH), Pohang 37673, Republic of Korea

<sup>c</sup> State Key Laboratory of Catalysis, Dalian Institute of Chemical Physics, Chinese Academy of Sciences, Dalian 116023, China

<sup>d</sup> Department of Chemistry, Sungkyunkwan University, Suwon 16419, Republic of Korea

## ARTICLE INFO

### Keywords:

Pt nano-particle

CeO<sub>2</sub> nano-patch

Low temperature water-gas shift reaction

Excess H<sub>2</sub>

In-situ diffuse reflectance infrared Fourier transform spectroscopy

## ABSTRACT

Pt/CeO<sub>2</sub> has gained much attention for their high activity in low-temperature (LT) water-gas shift (WGS) reaction. However, the inclusion of H<sub>2</sub> in the feed as in the practical reaction condition significantly degrades the LT-WGS activity of the Pt/CeO<sub>2</sub> catalysts. In this contribution, the activity of Pt/CeO<sub>2</sub> catalyst under the feed gas containing excess H<sub>2</sub> (20 vol% of H<sub>2</sub>) was enhanced more than three times by forming CeO<sub>2</sub> nano-patches on Pt nano-particles. Both in-situ diffuse reflectance infrared Fourier transform spectroscopy and density functional theory calculation results indicate that dissociated H<sub>2</sub> on the Pt nano-particle inhibits the activity of the Pt/CeO<sub>2</sub> catalysts by occupying the active sites (Pt nano-particle-CeO<sub>2</sub> interface). On the other hand, thin CeO<sub>2</sub> nano-patches on Pt nano-particle suppressed the H<sub>2</sub> dissociation. As a result, the WGS reactivity of the active Pt nano-particle-CeO<sub>2</sub> interface was less affected by H<sub>2</sub>, granting the catalysts the high activity under the practical reaction conditions.

## 1. Introduction

The main purpose of the water-gas shift (WGS) reaction is to produce H<sub>2</sub> by reacting CO and H<sub>2</sub>O ( $\text{CO} + \text{H}_2\text{O} = \text{CO}_2 + \text{H}_2$ ). Developing highly active catalyst in the low-temperature (LT) WGS reaction (< 300 °C) is especially important for the application in fuel cells [1–8]. Since the reaction rate is slow at low temperature, a large amount of catalysts should be used in practical WGS reactors [1,2]. However, commercial CuO/ZnO/Al<sub>2</sub>O<sub>3</sub> catalyst is pyrophoric in its inactive state, presenting safety concerns when used in large quantities [1,2]. Platinum-Group-Metals (PGMs) supported on CeO<sub>2</sub> (e.g. Pt/CeO<sub>2</sub> or Au/CeO<sub>2</sub>) could be the ideal candidate catalysts for the LT-WGS reaction, not only because they are highly active in the LT-WGS reaction but also because they are not pyrophoric [1,2,7,9–13].

While the active sites for the LT-WGS reaction on Pt/CeO<sub>2</sub> catalysts are known to be the atomically dispersed Pt<sup>2+</sup> or the interface between Pt nano-particle (NP) and CeO<sub>2</sub> [12–22], most of the mechanistic studies have been performed under the feed consisting of CO and H<sub>2</sub>O.

However, the excess amount of H<sub>2</sub> is always present in the feed under the practical operating conditions. While the inclusion of H<sub>2</sub> in the feed has been reported to hamper the LT-WGS reaction activities of metal-deposited catalysts as represented by the negative kinetic order with respect to H<sub>2</sub> [3,23–25], only little attempts have been made to solve the problem. In particular, we found that the inclusion of H<sub>2</sub> in the reactants reduced the WGS activity of Pt/CeO<sub>2</sub> catalyst by a factor of 6 in this study, which highlights the importance of the issue.

In this context, the development of PGM/CeO<sub>2</sub> catalysts maintaining the high activity in the LT-WGS reaction with the feed containing H<sub>2</sub> is essentially required. We hypothesized that by blocking the Pt NP surface with CeO<sub>2</sub> nano-patches, the inhibitory effect of H<sub>2</sub> on the LT-WGS reaction activity could be alleviated by suppressing the activation of H<sub>2</sub> on Pt NP. In this study, two different types of catalyst were prepared; (i) Pt NP/CeO<sub>2</sub> catalyst with Pt NP size smaller than 1.5 nm ('Pt NP/CeO<sub>2</sub>' catalyst) and (ii) Pt NP/CeO<sub>2</sub> catalyst with ~2 nm sized Pt NP partially covered by CeO<sub>2</sub> nano-patches ('CeO<sub>2</sub>/Pt NP/CeO<sub>2</sub>' catalyst). The latter one was prepared by applying the controlled reductive treatment, the

\* Corresponding author.

E-mail address: [dohkim@snu.ac.kr](mailto:dohkim@snu.ac.kr) (D.H. Kim).

<https://doi.org/10.1016/j.apcatb.2021.121038>

Received 16 October 2021; Received in revised form 11 December 2021; Accepted 21 December 2021

Available online 23 December 2021

0926-3373/© 2021 Elsevier B.V. All rights reserved.

simple post-synthetic method to modify catalysts' structure [11]. During the CeO<sub>2</sub> agglomeration induced by the controlled reductive treatment, CeO<sub>2</sub> nano-patches are expected to form on Pt NP [26]. Here, we prepared two types of CeO<sub>2</sub>/Pt NP/CeO<sub>2</sub> catalysts. (i) **CeO<sub>2</sub>/Pt NP/CeO<sub>2</sub> 700R** was prepared by reducing Pt/CeO<sub>2</sub> with H<sub>2</sub> at 700 °C. As a result, most of the Pt NP was covered by CeO<sub>2</sub> nano-patches in CeO<sub>2</sub>/Pt NP/CeO<sub>2</sub> 700 R. (ii) **CeO<sub>2</sub>/Pt NP/CeO<sub>2</sub> 700NC** was prepared by selectively reducing Pt/CeO<sub>2</sub> surface with H<sub>2</sub> at 250 °C and then thermally treating the sample with N<sub>2</sub> at 700 °C. Since N<sub>2</sub> cannot reduce CeO<sub>2</sub> bulk, the CeO<sub>2</sub> agglomeration occurred less severely. As a result, the Pt NP was less covered by ceria nano-patches. The catalytic activity in the LT-WGS reaction of Pt NP/CeO<sub>2</sub> catalyst significantly decreased when 20 vol% of H<sub>2</sub> was added to the feed. In contrast, CeO<sub>2</sub>/Pt NP/CeO<sub>2</sub> catalyst maintained its high activity in the LT-WGS reaction even in the presence of H<sub>2</sub>. Especially, under the feed containing CO, H<sub>2</sub>O, CO<sub>2</sub> and H<sub>2</sub> at 250 °C, the activity of CeO<sub>2</sub>/Pt NP/CeO<sub>2</sub> 700NC catalyst was higher than that of Pt NP/CeO<sub>2</sub> catalyst by a factor of 3.5. A detailed in-situ CO-DRIFTS analysis combined with HAADF-STEM imaging and DFT calculations were conducted to reveal the origin of such improvement in the LT-WGS reaction activity under the realistic condition.

## 2. Materials and methods

### 2.1. Catalyst synthesis

Pt was impregnated on CeO<sub>2</sub> (Rhodia, BET surface area of 135 m<sup>2</sup>/g) with the incipient wetness impregnation method with aqueous Pt (NH<sub>3</sub>)<sub>4</sub>(NO<sub>3</sub>)<sub>2</sub> solution (Sigma Aldrich, 99.99% grade, metal basis) as a metal precursor at room temperature. After impregnation, the catalysts were dried in an oven at 100 °C for 24 hr.

To prepare Pt NP/CeO<sub>2</sub> catalyst (with 2 wt% of Pt loading), the dried Pt/CeO<sub>2</sub> was oxidized under 15 vol% O<sub>2</sub>/N<sub>2</sub> at 500 °C for 2 h and reduced under 10 vol% H<sub>2</sub>/N<sub>2</sub> at 400 °C for 2 h. *In-situ* CO-DRIFTS spectra were collected for Pt/CeO<sub>2</sub> samples before and after the reductive treatment (experimental protocols to collect the DRIFTS spectra are provided below, and detailed explanations for the spectra are provided in Fig. S1). Before the reductive treatment, most Pt exist as the cationic Pt species (Fig. S1). However, after the reductive treatment (at 250 or 400 °C), all the cationic Pt species transformed into the metallic Pt species (Fig. S1). This indicates that the cationic Pt species are not stable under the reducing conditions. [27–30] Since we conducted the reaction test after the pretreatment with H<sub>2</sub> at 400 °C, we did not explore the activity of the oxidized Pt/CeO<sub>2</sub> catalyst in this study.

To prepare CeO<sub>2</sub>/Pt NP/CeO<sub>2</sub> 700NC catalyst (Pt loading, 2 wt%), the dried Pt/CeO<sub>2</sub> was oxidized at 500 °C for 2 hr, reduced at 250 °C for 2 hr, and then thermally treated with N<sub>2</sub> at 700 °C for 2 hr. To prepare CeO<sub>2</sub>/Pt NP/CeO<sub>2</sub> 700 R catalyst (Pt loading, 2 wt%), the dried Pt/CeO<sub>2</sub> was oxidized at 500 °C for 2 hr and then reduced at 700 °C for 2 hr.

To suppress the formation of Pt NP ( $\geq 1$  nm) in Pt/CeO<sub>2</sub>, the Pt loading was decreased to 0.5 wt% (Pt(0.5)/CeO<sub>2</sub>). Dried Pt(0.5)/CeO<sub>2</sub> was oxidized at 500 °C for 2 h and reduced at 400 °C for 2 h. Pt/ $\gamma$ -Al<sub>2</sub>O<sub>3</sub> (with 2 and 6 wt% of Pt) was also prepared by adopting the same method except for using alumina (Sasol, 250 m<sup>2</sup>/g) instead of CeO<sub>2</sub>. Dried Pt/ $\gamma$ -Al<sub>2</sub>O<sub>3</sub> sample was oxidized at 500 °C for 2 h and reduced at 400 °C for 2 h. For the control experiments, 2 and 5 wt% of CeO<sub>2</sub> was impregnated on the reduced Pt/ $\gamma$ -Al<sub>2</sub>O<sub>3</sub> (with 6 wt% of Pt) by the incipient wetness impregnation method with aqueous Ce(NO<sub>3</sub>)<sub>3</sub>·6H<sub>2</sub>O solution (Sigma Aldrich) as a Ce precursor at room temperature. Afterward, the sample was oxidized at 400 °C for 2 h. The flow rate was always kept at 100 mL/min at the ramping rate of 10 °C/min.

### 2.2. Diffuse reflectance infrared fourier transform spectroscopy (DRIFTS) study

*In-situ* DRIFTS experiments were conducted in a diffuse reflectance cell (Praying Mantis, Harrick) installed in a Fourier transform infrared

(FT-IR) spectrometer (iS-50, Thermo Fisher Scientific) with a MCT detector (32 scans, resolution of 4 cm<sup>-1</sup>). 10 vol% H<sub>2</sub>/N<sub>2</sub> or 20 vol% O<sub>2</sub>/H<sub>2</sub> or N<sub>2</sub> were used to pretreat the sample at 400 °C for 30 min. 2 vol% CO/N<sub>2</sub> was used for CO adsorption. Spectra were collected by using two different methods: (i) After the reductive or oxidative pretreatments, samples were purged with N<sub>2</sub> for another 30 min at 400 °C. After cooling the sample temperature to 50 °C under N<sub>2</sub>, background spectra were collected before CO adsorption. (ii) After the reductive pretreatment, the sample temperature was cooled to 50 °C under H<sub>2</sub> to collect the background spectra before CO adsorption under H<sub>2</sub>. The CO-FTIR spectra were collected after a brief purge with N<sub>2</sub> (or H<sub>2</sub>) to remove gas phase CO.

### 2.3. Transition electron microscopy (TEM)

High angle annular dark field-scanning transmission electron microscopy (HAADF-STEM) images were acquired on a spherical aberration-corrected scanning transmission electron microscope (JEM ARM-200 F, JEOL) at the National Center for Inter-University Research Facilities at Seoul National University.

To obtain the size distribution curves of the Pt NPs, more than 200 Pt NPs from several different HAADF-STEM images were counted with ImageJ software. Pt dispersion was estimated from size distribution curves according to the following equation: [31].

$$D(\%) = \frac{115.4}{d_p^{0.81}} \quad \text{and} \quad d_p = \left( \frac{\sum nd^3}{\sum nd^{2.15}} \right)^{1.23}$$

Here, D is the Pt dispersion (%),  $d_p$  is the average size of Pt NPs (nm),  $d$  is the diameter of Pt NPs (nm), and  $n$  is the number of Pt NPs with the diameter  $d$ .

### 2.4. Surface area measurement

N<sub>2</sub> adsorption/desorption isotherms were measured on a Micromeritics ASAP 2010 apparatus at the temperature of liquid N<sub>2</sub> (−196 °C). Before analysis, all catalysts were pretreated at 300 °C for 4 hr under vacuum condition.

### 2.5. CO chemisorption

CO chemisorption was performed on a BET-CAT-II (BEL Japan Inc.) at −78 °C to selectively adsorb CO on Pt following the reported protocols [32]. Briefly, 0.05 g of sample was reduced at 400 °C for 30 min under a 10 vol% H<sub>2</sub>/N<sub>2</sub> flow. After cooling to −78 °C under N<sub>2</sub>, CO pulses were introduced to the sample. CO chemisorption for CeO<sub>2</sub>/Pt NP/CeO<sub>2</sub> samples were also conducted after oxidation at 400 °C under a 5 vol% O<sub>2</sub>/He flow for 30 min and reduction at 150 °C under a 10 vol% H<sub>2</sub>/N<sub>2</sub> flow for 30 min (Section 3.2.3).

### 2.6. O<sub>2</sub> chemisorption

O<sub>2</sub> chemisorption was performed on a BET-CAT-II (BEL Japan Inc.) at 100 °C. After the reductive treatment at 400 °C with 10 vol% H<sub>2</sub>/N<sub>2</sub> for 30 min, samples were purged with He for another 30 min. After cooling the sample temperature to 100 °C, O<sub>2</sub> pulses (5 vol% O<sub>2</sub>/He in He flow) were introduced until adsorption reached saturation. 0.05 g of sample was used for the analysis. The amount of O<sub>2</sub> adsorbed on Pt was excluded based on the nominal Pt dispersion estimated from CO chemisorption at −78 °C to measure the amount of O<sub>2</sub> adsorbed on CeO<sub>2</sub>. Each Pt atom was assumed to adsorb one O atom (O/Pt = 1.0). [33].

### 2.7. X-ray photoelectron spectroscopy (XPS)

XPS analysis was conducted on a K-alpha instrument (Thermo VG, U. K.) with monochromated Al X-ray radiation (360 W). The charging effects were corrected with respect to the C 1 s binding energy at 284.5 eV.

[34].

## 2.8. Catalytic evaluation

The WGS reaction was performed in a fixed bed reactor at atmospheric pressure with 0.06 g of catalyst. The feed mixtures were prepared using mass flow controllers (MKS Instruments, Inc.). The reaction was conducted in the temperature range from 150 to 300 °C with the interval of 50 °C. The reactant mixture was composed of either (i) 3 vol % CO, 24 vol % H<sub>2</sub>O and 3 vol % CO<sub>2</sub> or (ii) 3 vol % CO, 24 vol % H<sub>2</sub>O, 3 vol % CO<sub>2</sub>, and 20 vol % H<sub>2</sub>. The total flow rate was 70 mL/min with He as the balance gas. The inlet and outlet gas streams were analyzed online using a TCD and a parallel gas chromatograph (GC, Younglin, Inc.) equipped with a Carboxen 1000 column and a flame ionization detector (FID). The CO conversion data were collected after reaching the steady-state at each temperature. Before the reaction, the catalysts were pretreated with 5 vol % H<sub>2</sub>/He at 400 °C for 1 hr. In addition, the WGS reaction rate at 250 °C over the exposed Pt atom on the catalysts and over the total Pt loading on the catalysts (2 wt%) was calculated by using the following formula:

WGS reaction rate over exposed Pt(or over total Pt loading)

$$\left( \frac{\text{moles of CO}}{\text{moles of Pt} \cdot \text{sec}} \right) = \frac{\text{CO conversion}(\%) \times \text{CO flow rate} \left( \frac{\text{mol}}{\text{sec}} \right)}{\text{Moles of exposed Pt (or mole of Pt loaded)} (\text{mol})}$$

In addition, the catalytic stability of CeO<sub>2</sub>/Pt NP/CeO<sub>2</sub> 700NC was investigated by performing the WGS reaction at 300 °C for 90 h under the full feed (Fig. S4). Sample was sieved to 150–180 μm size, and 0.05 g of sample was mixed with 0.3 g of α-Al<sub>2</sub>O<sub>3</sub>. CO<sub>2</sub> production was estimated by using mass spectrometry. The total flow rate was 100 mL/min.

## 2.9. Computational methods

Density functional theory (DFT) calculations were performed using Vienna ab initio simulation package (VASP).[35] Projector augmented wave (PAW) method was employed to efficiently replace the core electrons. Exchange-correlation energies were treated by Perdew-Burke-Ernzerhof (PBE) functional based on spin-polarized generalized gradient approximation (GGA). All energy calculations used a plane wave expansion with a cutoff energy of 400 eV. Brillouin zone was sampled with 2 × 2 × 1 k-grid within the scheme of Monkhorst and Pack for slab models. Dipole correction was employed to treat the physically spurious local potential induced by the use of asymmetric slab model. The localization of strongly correlated electrons and their unrealistic self-interaction in the conventional DFT calculations were accounted for by the DFT+U method.[36] The effective U value of 5.0 eV was added to correctly describe the 4f electrons of Ce ions.[37] The structures of considered models were geometrically optimized using conjugate gradient method with a maximum atomic force of < 0.03 eV/Å. Adsorption energy of an adsorbate molecule was calculated as

$$E_{\text{ads}} = E_{\text{adsorbate/slab}} - E_{\text{slab}} - E_{\text{adsorbate}}$$

where  $E_{\text{adsorbate/slab}}$ ,  $E_{\text{slab}}$ , and  $E_{\text{adsorbate}}$  are the total energies of a slab model with an adsorbate molecule, a slab model without an adsorbate molecule, and an isolated adsorbate molecule, respectively. CO and H<sub>2</sub> molecules were employed as adsorbates.

Pt<sub>10</sub>/CeO<sub>2</sub>(111) model was constructed by depositing a FCC-stacked Pt NP structure (Pt<sub>10</sub>) on p(3 × 3) surface unit cell of CeO<sub>2</sub>(111) to calculate  $E_{\text{ads}}$  of CO and H<sub>2</sub> molecules. The Pt NP structure was obtained from a literature where the Pt<sub>10</sub> NP structure was constructed by sequentially stacking Pt atoms on the lowest-energy adsorption sites. [38].

Vibrational frequencies of a CO molecule on metallic Pt and Pt oxide slab models were obtained by calculating the Hessian matrix of a CO molecule while fixing the slab models. For the Hessian matrix

calculation, central finite difference with two displacements of 0.04 Å was used. To investigate the variations in the CO-stretching frequency with respect to the charge state of Pt atoms, PtO(100), Pt<sub>2</sub>O(111) and Pt(111) slab models were constructed with reference to literatures on the relevant structure of the corresponding metal/oxygen ratio.[39–43].

## 3. Results and discussion

### 3.1. The LT-WGS reaction activity of differently prepared Pt/CeO<sub>2</sub> catalysts

Fig. 1 shows the LT-WGS reaction activities (at 250 °C) of Pt NP/CeO<sub>2</sub>, CeO<sub>2</sub>/Pt NP/CeO<sub>2</sub> 700NC and 700 R catalysts in the presence and absence of H<sub>2</sub>. The addition of H<sub>2</sub> significantly decreased the activity of Pt NP/CeO<sub>2</sub> catalyst; the CO conversion decreased from 60.8% to 11.3% (Fig. 1a). In other words, the reaction rate of Pt NP/CeO<sub>2</sub> decreased by 81% with the inclusion of H<sub>2</sub> in the feed. The activity of Pt NP/CeO<sub>2</sub> catalyst in the temperature range of 150–300 °C in the presence and absence of H<sub>2</sub> are compared in Fig. S2. On the contrary, the addition of H<sub>2</sub> less affected the activity of CeO<sub>2</sub>/Pt NP/CeO<sub>2</sub> 700NC catalyst; the CO conversion decreased from 47.0% to 37.1% (Fig. 1b). The reaction rate of CeO<sub>2</sub>/Pt NP/CeO<sub>2</sub> 700NC decreased by 21% with the inclusion of H<sub>2</sub> in the feed. Likewise, the activity of CeO<sub>2</sub>/Pt NP/CeO<sub>2</sub> 700 R catalyst was only slightly affected by the addition of H<sub>2</sub>; the CO conversion decreased from 12.9% to 11.3% (Fig. 1c). Under the H<sub>2</sub>-free feed, Pt NP/CeO<sub>2</sub> catalyst displayed superior activity to CeO<sub>2</sub>/Pt NP/CeO<sub>2</sub> 700NC catalyst (CO conversion; 60.8% vs 47.0%). However, the activity of CeO<sub>2</sub>/Pt NP/CeO<sub>2</sub> 700NC catalyst outperformed that of Pt NP/CeO<sub>2</sub> catalyst when H<sub>2</sub> was added to the feed (CO conversion; 37.1% vs 11.3%). The activity of Pt NP/CeO<sub>2</sub>, CeO<sub>2</sub>/Pt NP/CeO<sub>2</sub> 700NC and 700 R catalysts in the temperature range of 150–300 °C in the presence of H<sub>2</sub> are compared in Fig. S3. Both Pt NP/CeO<sub>2</sub> and CeO<sub>2</sub>/Pt NP/CeO<sub>2</sub> 700NC catalysts also displayed good stability under the feed with H<sub>2</sub> (Fig. S4). Note also that the deactivation resulting from the inclusion of H<sub>2</sub> in the feed is reversible; the catalytic activity recovered when H<sub>2</sub> was removed from the reactant feed (Fig. S5).

Note that the LT-WGS reaction below 300 °C is hardly limited by the thermodynamic constraint due to the presence of H<sub>2</sub> in the feed under the conditions used in this study (please refer to the supplementary discussion I in SI).[25,44,45] Therefore, the following two questions should be addressed to understand the catalytic behaviors of Pt/CeO<sub>2</sub> catalysts in Fig. 1: (i) Why the addition of H<sub>2</sub> decreased the LT-WGS reaction activity of Pt/CeO<sub>2</sub> catalysts? (ii) Why CeO<sub>2</sub>/Pt NP/CeO<sub>2</sub> catalysts were more resistant against H<sub>2</sub> addition? After characterizing the catalysts' structure with in-situ CO-DRIFTS spectra in Section 3.2 and discussing the active sites in Section 3.3, we will return to above questions in Section 3.4.

### 3.2. Identification of surface Pt sites on Pt NP/CeO<sub>2</sub>, CeO<sub>2</sub>/Pt NP/CeO<sub>2</sub> 700NC and 700 R catalysts with in-situ CO-DRIFTS spectra

#### 3.2.1. Comparison of in-situ CO-DRIFTS spectra of Pt NP/CeO<sub>2</sub>, CeO<sub>2</sub>/Pt NP/CeO<sub>2</sub> 700NC and 700 R catalysts

Performing in-situ analysis to study the reduced catalyst surfaces is important especially when studying samples that can be readily re-oxidized under mild conditions. For example, the reduced Pt NP can be re-oxidized when exposed to air at room temperature, which can have significant influence on the *ex-situ* characterization results.[46–48] The in-situ study is necessary to investigate Pt/CeO<sub>2</sub> since both Pt NP and reduced CeO<sub>2</sub> surface can be readily re-oxidized.[46,49] In this context, in-situ DRIFTS study with CO as a probe molecule is the effective approach since it can investigate the pre-reduced catalysts' surface with high surface sensitivity. Fig. 2a displays in-situ CO-DRIFTS spectra of Pt NP/CeO<sub>2</sub>, CeO<sub>2</sub>/Pt NP/CeO<sub>2</sub> 700NC and 700 R catalysts. The spectra of Pt NP/CeO<sub>2</sub> catalyst displayed three peaks centered at 1840, 2074 and 2090 cm<sup>−1</sup>. The peak at 1840 cm<sup>−1</sup> was assigned to the bridge-bonded

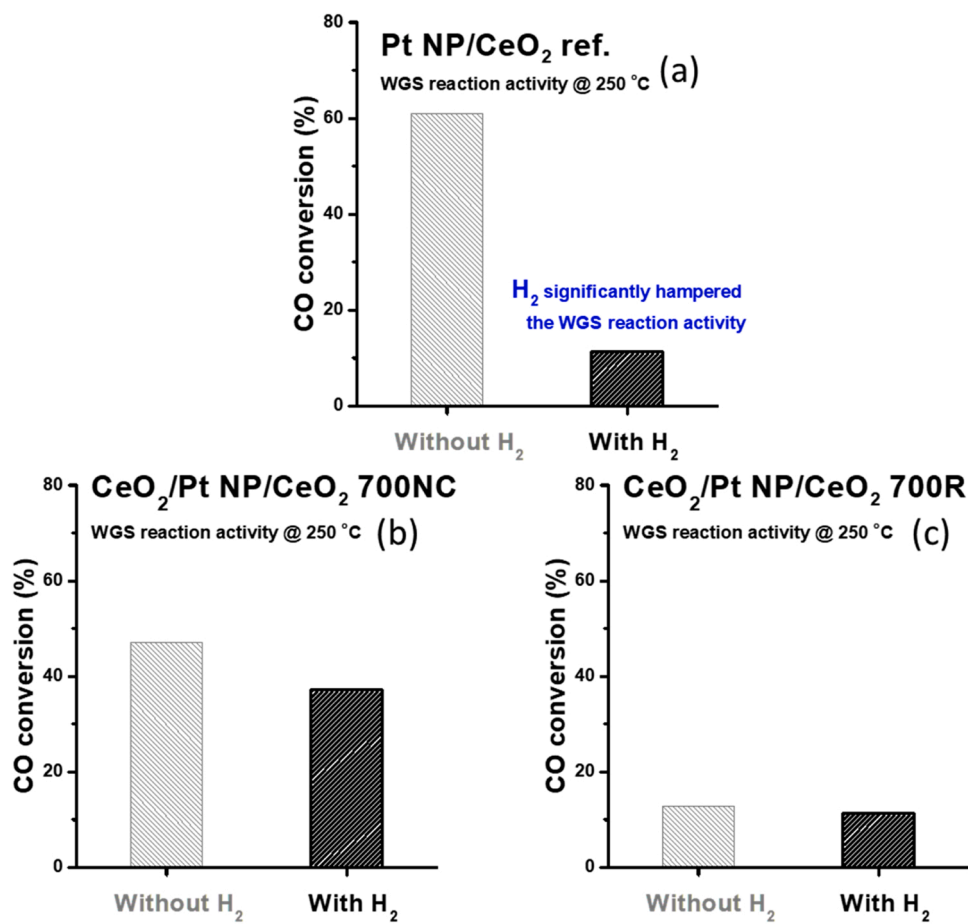


**Fig. 1.** The LT-WGS reaction activity at 250 °C of Pt NP/CeO<sub>2</sub> (a), CeO<sub>2</sub>/Pt NP/CeO<sub>2</sub> 700NC (b) and 700 R (c) catalysts in the presence and absence of H<sub>2</sub>. The catalytic activity was evaluated after the pretreatment with H<sub>2</sub> at 400 °C.

CO on Pt NP, while the main peak at 2074 cm<sup>-1</sup> and the shoulder peak at 2090 cm<sup>-1</sup> were assigned to the linear-bonded CO on undercoordinated and well-coordinated Pt NP, respectively.[28,50] On HAADF-STEM images of Pt NP/CeO<sub>2</sub> catalyst in Fig. 2b, the presence of Pt NP larger than 1 nm is clearly visible (more TEM images in Fig. S6). The Pt particle size distribution curves obtained from HAADF-STEM images in Fig. 2e show that the size of most of Pt NP on Pt NP/CeO<sub>2</sub> catalyst ranged from 1 to 2 nm.

Interestingly, CeO<sub>2</sub>/Pt NP/CeO<sub>2</sub> 700NC and 700 R catalysts displayed only small CO-DRIFTS peak at 2074 cm<sup>-1</sup>, but instead displayed the large CO-DRIFTS peaks centered at 2080 and 2090 cm<sup>-1</sup>, respectively (Fig. 2a). The size of Pt NP should be very large (> 17 nm) to possess dominantly the well-coordinated Pt sites represented by the CO-DRIFTS peak in the region of 2080–2090 cm<sup>-1</sup>. [50] However, the Pt NP larger than 10 nm in size is hardly observed on HAADF-STEM images of CeO<sub>2</sub>/Pt NP/CeO<sub>2</sub> 700NC and 700 R catalysts in Figs. 2c and 2d, respectively. (More TEM images of CeO<sub>2</sub>/Pt NP/CeO<sub>2</sub> 700 R and 700NC catalysts are provided in Fig. S7 and S8, respectively.) The average size of Pt NP is 2.1 and 3.2 nm in CeO<sub>2</sub>/Pt NP/CeO<sub>2</sub> 700NC and 700 R catalysts, respectively, according to the particle size distribution curves in Fig. 2e obtained from HAADF-STEM images (results are summarized in Table 1). This demonstrates that the CO-DRIFTS peaks in the region of 2080–2090 cm<sup>-1</sup> in Fig. 2a should not be assigned to CO adsorbed on well-coordinated Pt NP. Another interesting observation from Fig. 2a is that the spectra of CeO<sub>2</sub>/Pt NP/CeO<sub>2</sub> catalysts did not display the peaks at 1840 cm<sup>-1</sup> arising from the bridge-bonded CO on Pt NP (see the inset figure in Fig. 2a magnifying the spectra in the wavenumber region of 1800–1900 cm<sup>-1</sup>). The absence of bridge-bonded CO peak has often been considered as the evidence of the atomic distribution of Pt.[51]

However, this is not the case in the present study because the presence of Pt NP larger than 2 nm in high concentration is clearly observed in HAADF-STEM images of CeO<sub>2</sub>/Pt NP/CeO<sub>2</sub> 700NC and 700 R catalysts in Fig. 2c and d, respectively. Therefore, to utilize in-situ CO-DRIFTS spectra as a means to characterize the active sites on Pt/CeO<sub>2</sub> catalysts, we should (i) convincingly re-assign the shoulder peak at ~2090 cm<sup>-1</sup> and (ii) understand why CeO<sub>2</sub>/Pt NP/CeO<sub>2</sub> catalysts did not display the bridge-bonded CO peak at 1840 cm<sup>-1</sup>.

### 3.2.2. Assigning the CO-DRIFTS peak at ~2090 cm<sup>-1</sup>

Series of additional experiments were performed to assign the CO-DRIFTS peak at ~2090 cm<sup>-1</sup> observed on Pt NP/CeO<sub>2</sub> (Fig. 2a). First of all, Pt/CeO<sub>2</sub> with no Pt NP (≥ 1 nm) was prepared to compare its in-situ CO-DRIFTS spectra with those of Pt NP/CeO<sub>2</sub> catalyst. The Pt loading was decreased from 2 to 0.5 wt% to suppress the formation of Pt NP on CeO<sub>2</sub> (Pt(0.5)/CeO<sub>2</sub>). Time on stream in-situ CO-DRIFTS spectra of Pt(0.5)/CeO<sub>2</sub> sample in Fig. S9a demonstrate the absence of Pt NP (≥ 1 nm), since the shift in peak maxima of CO adsorbed on Pt by the lateral interaction was not observed.[51] On the contrary, the shift in peak maxima of CO adsorbed on Pt NP was clearly observed on in-situ CO-DRIFTS spectra of Pt NP/CeO<sub>2</sub> catalyst (Fig. S9b). In addition, the abundant atomically dispersed Pt could be observed in TEM images of Pt (0.5)/CeO<sub>2</sub> in Fig. S10. When comparing in-situ CO-DRIFTS spectra of Pt (0.5)/CeO<sub>2</sub> and Pt NP/CeO<sub>2</sub> samples, the peak at ~2090 cm<sup>-1</sup> was observed only on the latter one (Fig. 3a). Hence, the shoulder peak at ~2090 cm<sup>-1</sup> should be related to the presence of Pt NP (≥ 1 nm) on CeO<sub>2</sub> surface.

Previous studies on Pt surface, Pt/Al<sub>2</sub>O<sub>3</sub> and Pt/SiO<sub>2</sub> samples assigned the CO-DRIFTS peak at ~2090 cm<sup>-1</sup> to the linearly bonded CO

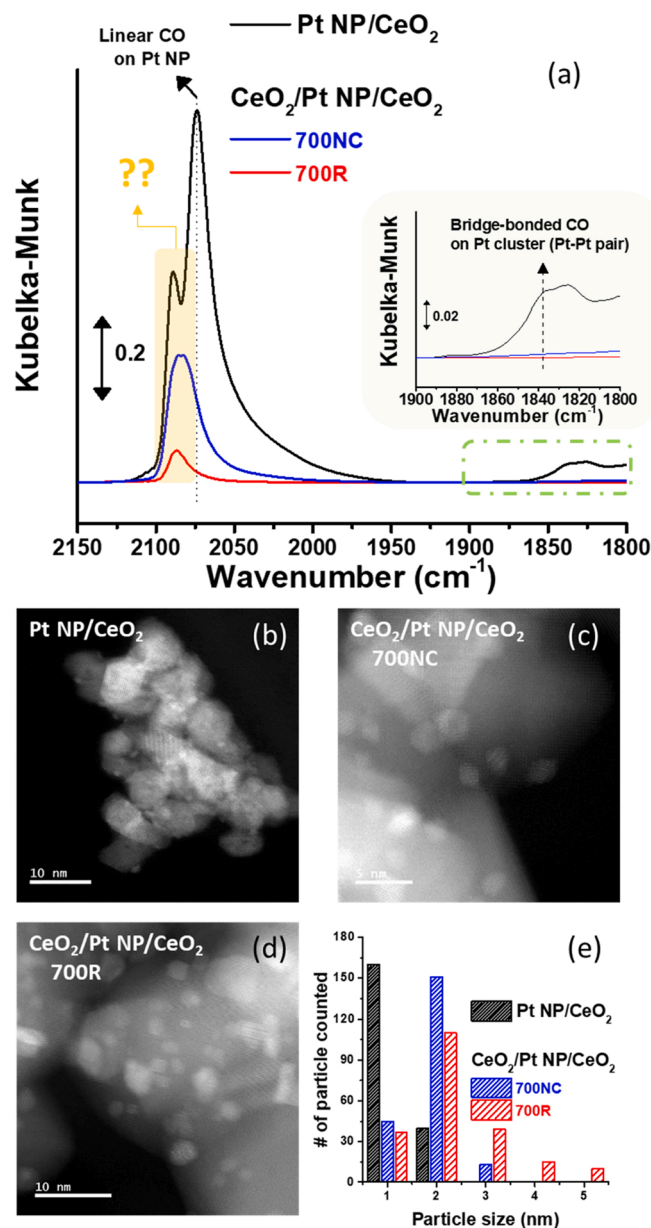


**Fig. 2.** (a) *In-situ* CO-DRIFTS spectra of Pt NP/CeO<sub>2</sub>, CeO<sub>2</sub>/Pt NP/CeO<sub>2</sub> 700NC and 700 R catalysts collected after the pretreatment with H<sub>2</sub> at 400 °C followed by the CO adsorption at 50 °C for 1 hr. The inset figure magnifies the spectra in the wavenumber region of 1800–1900 cm<sup>-1</sup>. HAADF-STEM images of Pt NP/CeO<sub>2</sub> (b), CeO<sub>2</sub>/Pt NP/CeO<sub>2</sub> 700NC (c) and 700 R (d) catalysts, and (e) their Pt NP size distribution curves.

on well-coordinated Pt NP, which exists abundantly on large-sized Pt NP [50,52–54]. The size distribution curves of Pt NP on Pt NP/CeO<sub>2</sub> and Pt (2 wt%)/ $\gamma$ -Al<sub>2</sub>O<sub>3</sub> samples were obtained from their HAADF-STEM images in Fig. S6 and S11, respectively. According to the size distribution curves in Fig. S12, the average size of Pt NP on Pt/ $\gamma$ -Al<sub>2</sub>O<sub>3</sub> and Pt NP/CeO<sub>2</sub> samples are 1.6 and 1.5 nm, respectively (summarized in Table 1). Fig. 3b compares the *in-situ* CO-DRIFTS spectra of Pt/ $\gamma$ -Al<sub>2</sub>O<sub>3</sub> and Pt NP/CeO<sub>2</sub> samples. Although the average size of Pt NP on both samples is similar (1.6 vs 1.5 nm), the intensity of the peak at ~2090 cm<sup>-1</sup> is much higher on Pt NP/CeO<sub>2</sub> sample. This indicates that the shoulder peak at ~2090 cm<sup>-1</sup> may not originate from CO adsorbed on well-coordinated Pt NP. Such conclusion agrees with the results obtained from the CO-DRIFTS spectra of CeO<sub>2</sub>/Pt NP/CeO<sub>2</sub> 700NC and 700 R catalysts in Fig. 2a. It should also be pointed out that atomically

dispersed Pt was observed on the HAADF-STEM images of Pt NP/CeO<sub>2</sub> catalyst in addition to Pt NP (Fig. S6d). However, as discussed in Fig. 3a, the presence of the atomically dispersed Pt on CeO<sub>2</sub> does not contribute to the shoulder peak at ~2090 cm<sup>-1</sup>.

CeO<sub>2</sub> was loaded on Pt/ $\gamma$ -Al<sub>2</sub>O<sub>3</sub> to form the Pt NP-CeO<sub>2</sub> interface in order to assign the shoulder peak at ~2090 cm<sup>-1</sup>. *In-situ* CO-DRIFTS spectra were collected after loading 2 and 5 wt% of CeO<sub>2</sub> on Pt(6 wt %)/ $\gamma$ -Al<sub>2</sub>O<sub>3</sub> sample. To prevent the Pt sintering, the treatment temperature to decompose Ce(NO<sub>3</sub>)<sub>3</sub>·6 H<sub>2</sub>O precursor (400 °C) was lower than the treatment temperature of Pt/ $\gamma$ -Al<sub>2</sub>O<sub>3</sub> sample (500 °C). After loading CeO<sub>2</sub>, the main peak from the linearly adsorbed CO on undercoordinated Pt NP slightly shifted to the higher wavenumber (from 2063 to 2066 and 2068 cm<sup>-1</sup>, Fig. 3c). This is understandable since the peak maximum from the linearly bonded CO on undercoordinated Pt NP was observed at the higher wavenumber in Pt NP/CeO<sub>2</sub> sample than in Pt/ $\gamma$ -Al<sub>2</sub>O<sub>3</sub> sample (2074 vs 2065 cm<sup>-1</sup>, Fig. 3b). To observe the variation in the peak intensity in the region of 2070–2090 cm<sup>-1</sup>, the peak maxima of the main peak of CeO<sub>2</sub>/Pt/ $\gamma$ -Al<sub>2</sub>O<sub>3</sub> samples were shifted to match that of Pt/ $\gamma$ -Al<sub>2</sub>O<sub>3</sub> sample (Fig. S13). The peak intensity in the region of 2070–2090 cm<sup>-1</sup> gradually increased when the CeO<sub>2</sub> loading increased from 0 to 2 and 5 wt% (Fig. 3c and S13). Therefore, the formation of the Pt NP-CeO<sub>2</sub> interface would bring about the DRIFTS peak in the region of 2070–2090 cm<sup>-1</sup>. Note also that the peak intensity in the region of 2070–2090 cm<sup>-1</sup> in Fig. S13 is smaller than that of Pt NP/CeO<sub>2</sub> in Fig. 2a. This might be attributed to the differences in spatial correlation and interaction between Pt NP and CeO<sub>2</sub> in Pt NP/CeO<sub>2</sub> and CeO<sub>2</sub>/Pt/ $\gamma$ -Al<sub>2</sub>O<sub>3</sub> samples.

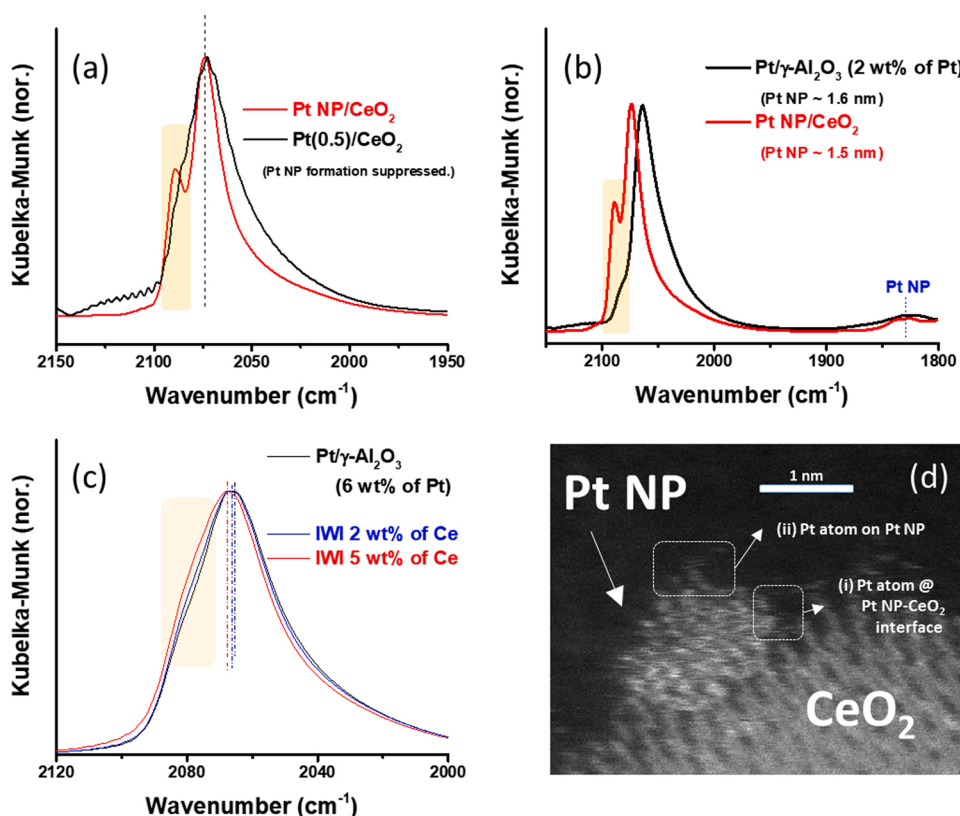
Fig. 3d displays the high resolution HAADF-STEM image of Pt NP (1.5 nm in diameter) supported on CeO<sub>2</sub> surface. When Pt NP is loaded on CeO<sub>2</sub> surface, two types of Pt sites would be formed; (i) the Pt atoms in direct contact with CeO<sub>2</sub> at the Pt-CeO<sub>2</sub> interface, and (ii) the Pt atoms not in contact with CeO<sub>2</sub> (Fig. 3d). Since the peak in the region of 2070–2090 cm<sup>-1</sup> increased in intensity with the formation of Pt NP-CeO<sub>2</sub> interface (Fig. 3c), we believe that the peak at 2090 cm<sup>-1</sup> should be assigned to the CO adsorbed on Pt atoms at the Pt NP-CeO<sub>2</sub> interface. Note also that the CO adsorption peak at 2090 cm<sup>-1</sup> is located in between the CO adsorption peaks on cationic and metallic Pt species, which appear at 2105 and 2075 cm<sup>-1</sup>, respectively (Fig. S1). DFT calculation was performed to correlate the charge state of Pt and the vibrational frequency of CO adsorbed on Pt. Fig. S14 shows that as the Pt surface becomes cationic, the vibrational frequency of CO adsorbed on Pt shifted to the higher wavenumber. Therefore, it could be inferred from DFT calculation results that the Pt atoms at the Pt NP-CeO<sub>2</sub> interface would become partially cationic by electronically interacting with CeO<sub>2</sub>. The O atoms of CeO<sub>2</sub> at the interface would withdraw electrons from Pt NP. In agreement with the present proposal, Blanchard et al. assigned the infrared peak at 2096 cm<sup>-1</sup> to the CO adsorbed on Pt<sup>δ+</sup> atoms resulting from the local Pt oxidation at the Pt NP-CeO<sub>2</sub> interface.[55] Libuda et al. also reported that the infrared peak from CO adsorbed at the periphery of Pt NP supported on CeO<sub>2</sub>(111) appears as the blue-shifted shoulder peak at 2090 cm<sup>-1</sup> by interacting with the spillover oxygen from CeO<sub>2</sub>. [56] As Vayssilov et al. pointed out, infrared technique should be combined with other approaches to identify the actual state of Pt species.[57] In this study, through combined studies, we could strictly assign the CO-DRIFTS peak at ~2090 cm<sup>-1</sup> to the CO adsorbed at the periphery of Pt NP supported on CeO<sub>2</sub> surface.

### 3.2.3. Identifying the structure of CeO<sub>2</sub>/Pt NP/CeO<sub>2</sub> 700NC and 700 R catalysts

Only the CO adsorption peak at ~2090 cm<sup>-1</sup> is observed on *in-situ* CO-DRIFTS spectra of CeO<sub>2</sub>/Pt NP/CeO<sub>2</sub> 700NC and 700 R catalysts (Fig. 4a, replotted from Fig. 2a). Based on the series of discussions in Sections 3.2.1 and 3.2.2, the peak at ~2090 cm<sup>-1</sup> was assigned to the CO adsorbed on Pt atoms at the Pt NP-CeO<sub>2</sub> interface. Hence, the CO-DRIFTS spectra in Fig. 4a indicate that CeO<sub>2</sub>/Pt NP/CeO<sub>2</sub> 700NC and 700 R catalysts are exclusively exposing the Pt NP-CeO<sub>2</sub> interface. A

**Table 1**BET surface area, pore volume, Pt dispersion and average Pt NP size of Pt/ $\gamma$ -Al<sub>2</sub>O<sub>3</sub>, Pt NP/CeO<sub>2</sub>, CeO<sub>2</sub>/Pt NP/CeO<sub>2</sub> 700NC and 700 R samples.

Sample	Surface area (m <sup>2</sup> /g) <sup>a</sup>	Pore volume (cm <sup>3</sup> /g) <sup>b</sup>	Pt dispersion from TEM images (%) <sup>c</sup>	Average Pt NP size from TEM images (nm) <sup>c</sup>	Pt dispersion from CO chemisorption (%) <sup>d</sup>	'Nominal' average Pt NP size from CO chemisorption (nm) <sup>d</sup>
Pt NP/CeO <sub>2</sub>	125	0.27	82	1.5	61	2.2
CeO <sub>2</sub> /Pt NP/CeO <sub>2</sub> 700NC	58	0.25	63	2.1	12	16.4
CeO <sub>2</sub> /Pt NP/CeO <sub>2</sub> 700 R	45	0.27	45	3.2	3	> 100
Pt/ $\gamma$ -Al <sub>2</sub> O <sub>3</sub> (2 wt % of Pt)	219	0.43	79	1.6	54	2.5

<sup>a</sup> From N<sub>2</sub> adsorption branch, BET.<sup>b</sup> From N<sub>2</sub> desorption branch, BJH.<sup>c</sup> From particle size distribution curves obtained from HAADF STEM images,  $d_p = (\Sigma nd^3 / \Sigma nd^{2.19})^{1.23}$ ,  $D (\%) = 115.4 / d_p^{0.81}$ .<sup>d</sup> From CO chemisorption at -78 °C.

**Fig. 3.** *In-situ* CO-DRIFTS spectra of Pt(0.5)/CeO<sub>2</sub> and Pt/ $\gamma$ -Al<sub>2</sub>O<sub>3</sub> (2 wt% of Pt) samples were compared to that of Pt NP/CeO<sub>2</sub> in (a) and (b), respectively. (c) *In-situ* CO-DRIFTS spectra were collected after loading 2 and 5 wt% of Ce on Pt/ $\gamma$ -Al<sub>2</sub>O<sub>3</sub> with 6 wt% of Pt. Spectra in (a), (b) and (c) were collected after the pretreatment with H<sub>2</sub> at 400 °C followed by the CO adsorption at 50 °C for 1 h ((a) and (b)) or 10 min ((c)). The peak CO band intensities in (a), (b) and (c) were normalized to compare the distribution of Pt species. (d) HR-HAADF-STEM image of Pt NP/CeO<sub>2</sub> showing the possible CO adsorption sites.

question arises about how the catalysts can expose only the interface without exposing the CO adsorption sites on under- or well-coordinated Pt NP.

The nominal Pt dispersion of CeO<sub>2</sub>/Pt NP/CeO<sub>2</sub> 700NC and 700 R catalysts was estimated from either Pt NP size distribution curves in Fig. 2e or CO chemisorption. The Pt dispersion of CeO<sub>2</sub>/Pt NP/CeO<sub>2</sub> 700NC and 700 R catalysts were estimated to be 63% and 45% from Pt NP size distribution curves, respectively, while those were estimated to be 12% and 3% from CO chemisorption, respectively (Fig. 4b and Table 1). Such large discrepancy indicates that most of Pt NP are covered by CeO<sub>2</sub> on both catalysts. The CeO<sub>2</sub> nano-patches formed on Pt NP would have inhibited the formation of the linear-bonded CO or the bridge-bonded CO on Pt NP (Fig. 4a). Alternatively, the CeO<sub>2</sub> nano-patches may have formed the interface with Pt NP to give the CO band at ~2090 cm<sup>-1</sup> (Fig. 4a). Indeed, the Pt NPs partially covered by CeO<sub>2</sub> nano-patches could be found at the periphery of CeO<sub>2</sub> particle in HR-HAADF-STEM images of CeO<sub>2</sub>/Pt NP/CeO<sub>2</sub> 700NC (Fig. 4c and S15). Note that while CO-DRIFTS spectra indicate that CeO<sub>2</sub>/Pt NP/CeO<sub>2</sub>

700NC exposes the larger Pt NP-CeO<sub>2</sub> interface than CeO<sub>2</sub>/Pt NP/CeO<sub>2</sub> 700 R (Fig. 4a), and that Pt NP interacting with CeO<sub>2</sub> would become cationic as predicted from DFT calculation (Fig. S14), the XP spectra could not clearly distinguish the oxidation state of Pt in these two samples. XP spectra indicate that Pt exists mostly as metallic in both samples (Fig. S16). This is understandable since XPS analysis is relatively less surface sensitive than DRIFTS analysis and much of Pt NP surface in both catalysts is covered with CeO<sub>2</sub> nano-patches. While CO-DRIFTS analysis characterizes the oxidation state of the accessible Pt atoms on the surface, XPS analyzes the average oxidation state of Pt within a few nm-depth from the sample surface. In addition, it would be worth to discuss whether the formation of CeO<sub>2</sub> nano-patches on Pt NP is related to Strong-Metal-Support-Interaction (SMSI) phenomena. SMSI phenomena can be defined as the reversible loss of the CO adsorption ability of PGM NP supported on reducible oxides after the reductive treatment at high temperature [58]. Under the reducing condition, reducible oxide with oxygen vacancy (OV) migrate onto PGM NP surface to minimize the surface energy [59,60]. As a result, the CO adsorption

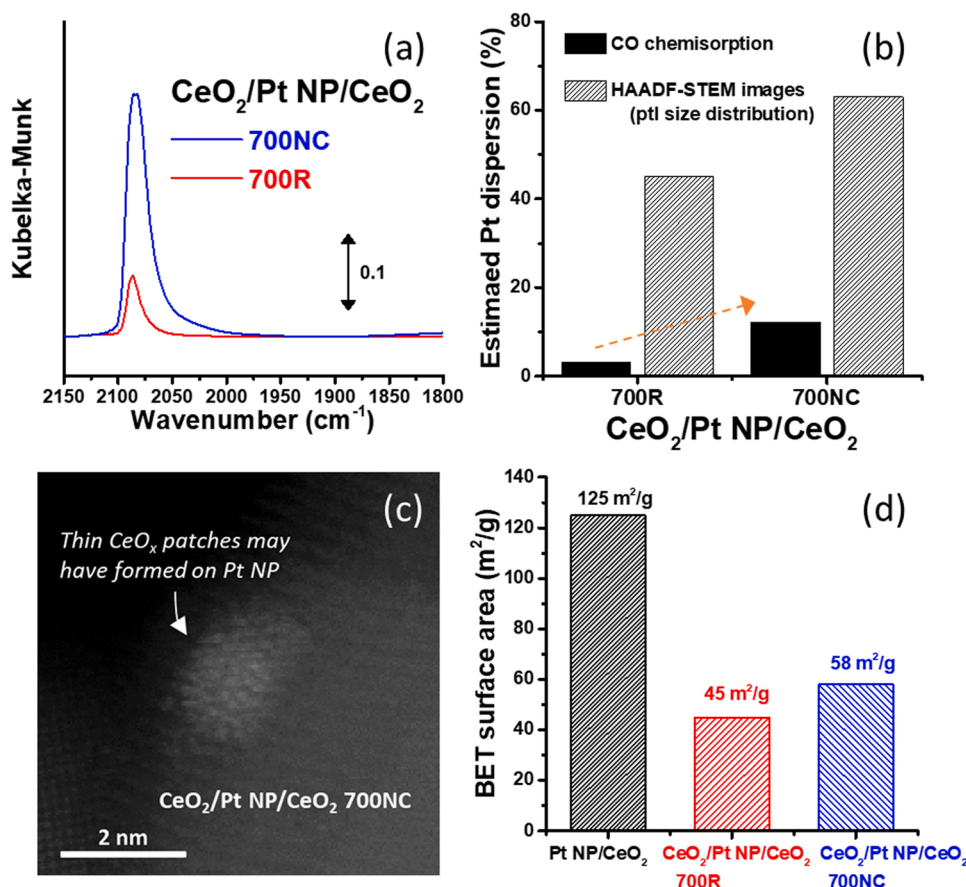
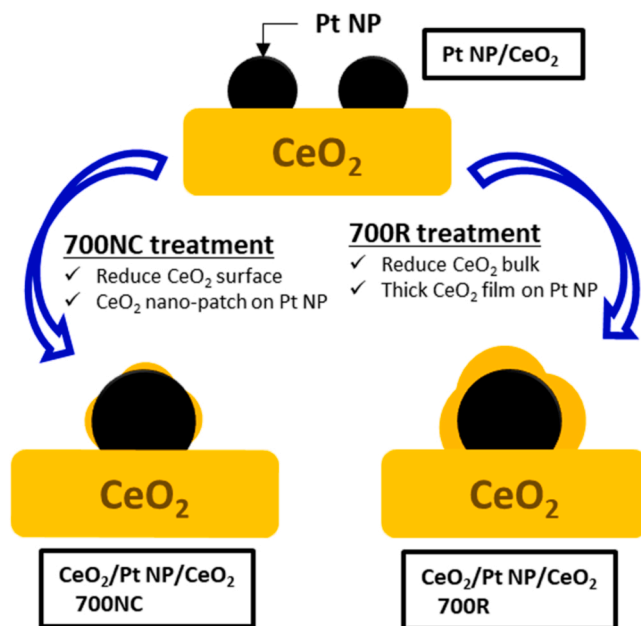


**Fig. 4.** (a) *In-situ* CO-DRIFTS spectra of CeO<sub>2</sub>/Pt NP/CeO<sub>2</sub> 700NC and 700 R catalysts collected after the pretreatment with H<sub>2</sub> at 400 °C followed by the CO adsorption at 50 °C for 1 h. For comparison, the CO-DRIFTS spectra in Fig. 2a are displayed again in (a). (b) The nominal Pt dispersions of CeO<sub>2</sub>/Pt NP/CeO<sub>2</sub> 700NC and 700 R catalysts estimated from CO chemisorption and particle size distribution curves obtained from HAADF-STEM images are compared. (c) HR-HAADF-STEM image of CeO<sub>2</sub>/Pt NP/CeO<sub>2</sub> 700NC. The Pt NP located at the periphery of CeO<sub>2</sub> particle is displayed in the figure. (d) BET surface area of Pt NP/CeO<sub>2</sub>, CeO<sub>2</sub>/Pt NP/CeO<sub>2</sub> 700 R and 700NC catalysts.

ability of PGM NP is suppressed under the reducing condition. However, when the OV's are replenished under the oxidizing condition at high temperature (e.g., 400 °C), reducible oxides retrieve from the PGM NP, and the CO adsorption ability of PGM NP is restored [59,60]. To verify whether the formation of CeO<sub>2</sub> nano-patches on Pt NP is related to SMSI phenomena, the CO adsorption ability of CeO<sub>2</sub>/Pt NP/CeO<sub>2</sub> 700 R and 700NC catalysts were investigated after the oxidative treatment at 400 °C. Table S1 shows that the oxidative treatment at 400 °C has no effect on the CO adsorption abilities of CeO<sub>2</sub>/Pt NP/CeO<sub>2</sub> 700 R and 700NC catalysts. Since the suppression of CO adsorption ability is not reversible, the formation of CeO<sub>2</sub> nano-patches on Pt NP may not be related to SMSI. Instead, CeO<sub>2</sub> nano-patches may have formed on Pt NP during the CeO<sub>2</sub> aggregation and structure modification [11].

CeO<sub>2</sub>/Pt NP/CeO<sub>2</sub> 700NC chemisorbed the larger amount of CO than CeO<sub>2</sub>/Pt NP/CeO<sub>2</sub> 700 R (0.28 vs 0.07 cm<sup>3</sup>/g, Fig. 4b). The former one also displayed the higher peak intensity at ~2090 cm<sup>-1</sup> in the CO-DRIFTS spectra (Fig. 4a). These observations indicate that the larger amount of Pt NP-CeO<sub>2</sub> interface is formed on CeO<sub>2</sub>/Pt NP/CeO<sub>2</sub> 700NC than on CeO<sub>2</sub>/Pt NP/CeO<sub>2</sub> 700 R. Such difference would be caused by the different heat treatments used to prepare each catalyst. The 700 R treatment used to prepare CeO<sub>2</sub>/Pt NP/CeO<sub>2</sub> 700 R reduces CeO<sub>2</sub> bulk to accelerate the CeO<sub>2</sub> agglomeration. [26] On the other hand, the 700NC treatment used to prepare CeO<sub>2</sub>/Pt NP/CeO<sub>2</sub> 700NC cannot reduce CeO<sub>2</sub> bulk. [26] For this reason, the BET surface area of the latter sample was higher than that of the former sample (58 vs 45 m<sup>2</sup>/g, Fig. 4d). After 700 R treatment, where structure destruction is severe, thick CeO<sub>2</sub> over-layers would block the Pt NP surface rather than forming the interface with Pt NP. On the contrary, after 700NC treatment, thin CeO<sub>2</sub> nano-patches would form the interface with Pt NP. The transformation of the surface structures of Pt NP/CeO<sub>2</sub> to CeO<sub>2</sub>/Pt NP/CeO<sub>2</sub> catalysts by 700NC or 700 R treatments is schematically illustrated in Scheme 1.



**Scheme 1.** Schematic illustration of the transformation of Pt NP/CeO<sub>2</sub> into CeO<sub>2</sub>/Pt NP/CeO<sub>2</sub> 700NC and 700 R catalysts.

### 3.3. Pt NP-CeO<sub>2</sub> interface catalyzes the LT-WGS reaction

Fig. 5a compares *in-situ* CO-DRIFTS spectra of Pt NP/CeO<sub>2</sub> and CeO<sub>2</sub>/Pt NP/CeO<sub>2</sub> 700 R catalysts collected after CO adsorption at 50 °C for 1 hr in the presence of H<sub>2</sub>. The peak intensity at ~2090 cm<sup>-1</sup>,

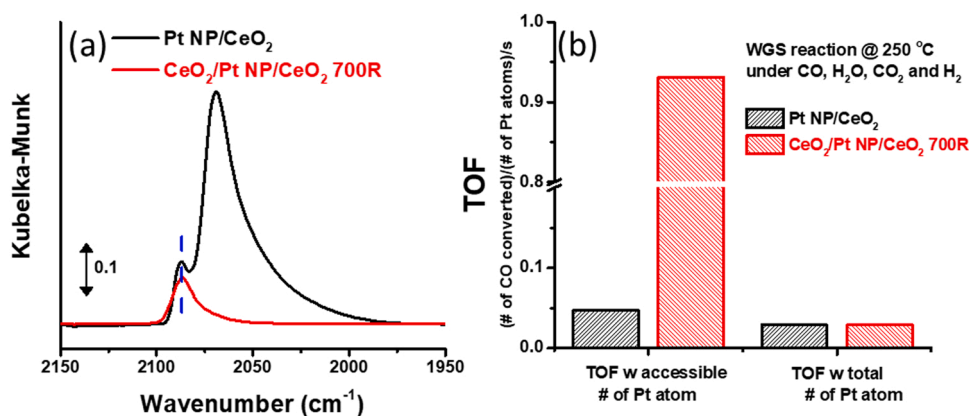


**Fig. 5.** (a) *In-situ* CO-DRIFTS spectra of Pt NP/CeO<sub>2</sub> and CeO<sub>2</sub>/Pt NP/CeO<sub>2</sub> 700 R catalysts, collected after the pretreatment with H<sub>2</sub> at 400 °C followed by the CO adsorption at 50 °C for 1 hr in the presence of H<sub>2</sub>. (b) TOF of Pt NP/CeO<sub>2</sub> and CeO<sub>2</sub>/Pt NP/CeO<sub>2</sub> 700 R catalysts were estimated over the number of Pt sites exposed on the surface (from CO chemisorption at −78 °C) and over the total amount of Pt loaded on the catalysts (2 wt%).

assigned to CO adsorbed on the Pt atoms at the Pt NP-CeO<sub>2</sub> interface, are similar on both catalysts (Fig. 5a). On the other hand, the peak at 2070 cm<sup>-1</sup>, which could be assigned to CO adsorbed on under-coordinated Pt NP, was observed only on Pt NP/CeO<sub>2</sub> but not on CeO<sub>2</sub>/Pt NP/CeO<sub>2</sub> 700 R (Fig. 5a). Therefore, in addition to Pt sites at the Pt NP-CeO<sub>2</sub> interface, Pt sites not interacting with CeO<sub>2</sub> would also exist on Pt NP/CeO<sub>2</sub>. However, the abundance of boundary sites should not be judged solely by the band intensity at ~2090 cm<sup>-1</sup>. This is because the intensity of the CO-DRIFTS peak at ~2090 cm<sup>-1</sup> could be influenced by the dynamic dipole coupling with CO adsorbed on under-coordinated Pt NP, given that CO species at the boundary and on the terrace are adjacent on the surface and also close in frequency.

The vast number of previous reports have shown that the Pt NP-CeO<sub>2</sub> interface would catalyze the LT-WGS reaction in Pt/CeO<sub>2</sub> catalyst. [12–17,22,24,61–66] For example, Stephanopoulos et al. reported in their series of publications that the metallic Pt NP on CeO<sub>2</sub> is the spectator species in the LT-WGS reaction. [14,61,62] Efstathiou et al. studied the LT-WGS reaction mechanism of Pt/CeO<sub>2</sub> catalysts by steady-state isotopic transient kinetic analysis (SSITKA) coupled with *in-situ* DRIFTS experiments, and concluded that the LT-WGS reaction proceed via the dual-site mechanism where CO adsorbed on Pt at the Pt-CeO<sub>2</sub> interface reacts with OH groups on the CeO<sub>2</sub> surface. [16,22,64] Likewise, Rodriguez et al. reported in their series of publications with the inverted catalysts that the interface between PGM and CeO<sub>2</sub> has the high catalytic activity in LT-WGS reaction. [17,65,66] Fig. 5b compares Turnover rates (TOF) of Pt NP/CeO<sub>2</sub> and CeO<sub>2</sub>/Pt NP/CeO<sub>2</sub> 700 R catalysts calculated over the exposed Pt sites (estimated from CO chemisorption at −78 °C) and over the total Pt loading on the catalysts (2 wt %). The WGS activities of the catalysts were evaluated under the feed of CO, H<sub>2</sub>O, CO<sub>2</sub> and H<sub>2</sub> at 250 °C. The TOF over the exposed Pt sites is much higher on CeO<sub>2</sub>/Pt NP/CeO<sub>2</sub> 700 R than on Pt NP/CeO<sub>2</sub> (0.93 vs 0.03 1/s, Fig. 5b). On the other hand, the TOF over the total Pt loading was the same for both catalysts (0.03 1/s, Fig. 5b). Such a huge discrepancy could be rationalized by considering that the TOF over the exposed Pt sites on Pt NP/CeO<sub>2</sub> would be significantly underestimated because of the presence of inactive Pt sites that are not interacting with CeO<sub>2</sub> (Fig. 5a). In addition, it would be worth to mention that the TOF over the exposed Pt sites of CeO<sub>2</sub>/Pt NP/CeO<sub>2</sub> 700 R, which is 0.93, is very high among Pt-based catalysts supported on various metal oxides reported in the literature (Table S2). [6,67–70].

It would be also interesting to discuss how the different OV concentration of Pt NP/CeO<sub>2</sub>, CeO<sub>2</sub>/Pt NP/CeO<sub>2</sub> 700 R and 700NC catalysts may affect the WGS activity. The main role of OV on Pt/CeO<sub>2</sub> catalysts in the WGS reaction is to activate H<sub>2</sub>O molecule. [15,22] The number of OV on the catalysts' surface was estimated by O<sub>2</sub> chemisorption and it was compared to the number of exposed Pt sites measured by CO

chemisorption (Table S3). 0.086, 0.028 and 0.037 mmol/g of O<sub>2</sub> chemisorbed on Pt NP/CeO<sub>2</sub>, CeO<sub>2</sub>/Pt NP/CeO<sub>2</sub> 700 R and 700NC catalysts, respectively (Table S3). On the other hand, 0.063, 0.003 and 0.012 mmol/g of CO chemisorbed on Pt NP/CeO<sub>2</sub>, CeO<sub>2</sub>/Pt NP/CeO<sub>2</sub> 700 R and 700NC catalysts, respectively (Table S3). Here, the number of OV on the catalysts' surface can be calculated by assuming that each of the exposed Pt atom and the OV on ceria surface chemisorb one O atom. The ratio between the number of OV to the number of exposed Pt sites was 1.7, 17.5 and 5.2 on Pt NP/CeO<sub>2</sub>, CeO<sub>2</sub>/Pt NP/CeO<sub>2</sub> 700NC and 700 R catalysts, respectively (Table S3). In all catalysts, the ratio between the number of OV to the number of exposed Pt sites was larger than 1.0. The ratio between the number of OV to the number of exposed Pt sites was close to 1.0 on Pt NP/CeO<sub>2</sub>. However, considering that much of Pt in Pt NP/CeO<sub>2</sub> catalyst does not form the interface with the ceria surface, the number of OV would be much larger than that of active sites at the interface. Since abundant OV exist on the catalysts studied in this work (Table S3), the difference in the surface concentration of OV may have minor influence on the WGS activity.

As demonstrated in Section 3.1, the purpose of this study is to investigate how H<sub>2</sub> deactivates the Pt NP/CeO<sub>2</sub> catalyst's LT-WGS reaction activity, and to understand why CeO<sub>2</sub>/Pt NP/CeO<sub>2</sub> catalysts' LT-WGS reaction activities were maintained upon the addition of H<sub>2</sub> to the reactant feed. Now, we have the important clue to understand the phenomena; the catalytically active Pt NP-CeO<sub>2</sub> interface could be identified by *in-situ* CO-DRIFTS spectra. In the next section, we collected *in-situ* CO-DRIFTS spectra of Pt NP/CeO<sub>2</sub>, CeO<sub>2</sub>/Pt NP/CeO<sub>2</sub> 700NC and 700 R catalysts both in the presence and absence of H<sub>2</sub> in the reactant feed to understand how the CO adsorption on the Pt NP-CeO<sub>2</sub> interface is affected by H<sub>2</sub>.

#### 3.4. Investigation of how CO adsorption at the Pt NP-CeO<sub>2</sub> interface on Pt NP/CeO<sub>2</sub>, CeO<sub>2</sub>/Pt NP/CeO<sub>2</sub> 700NC and 700R catalysts is affected by H<sub>2</sub>

##### 3.4.1. The case of Pt NP/CeO<sub>2</sub> catalyst

Fig. 6a compares *in-situ* CO-DRIFTS spectra of Pt NP/CeO<sub>2</sub> catalysts collected after CO adsorption at 50 °C for 1 h in the presence and absence of H<sub>2</sub>. When H<sub>2</sub> was added to the feed, the bridge-bonded CO peak at 1840 cm<sup>-1</sup> disappeared (inset of Fig. 6a) and the CO adsorption peak at ~2074 and ~2090 cm<sup>-1</sup> greatly decreased in intensity (Fig. 6a). In other words, the presence of H<sub>2</sub> hampered the CO adsorption on Pt NP. In order to understand how CO and H<sub>2</sub> molecules would interact with Pt NP, DFT calculation was performed (Fig. 6b and c). After constructing Pt<sub>10</sub>/CeO<sub>2</sub>(111) model with reference to literatures, CO and H<sub>2</sub> molecules were adsorbed on Pt NP. Of the calculations performed, only the most stable energies are displayed. Fig. 6b shows that the dissociative adsorption of H<sub>2</sub> is favored over the molecular adsorption of H<sub>2</sub> on

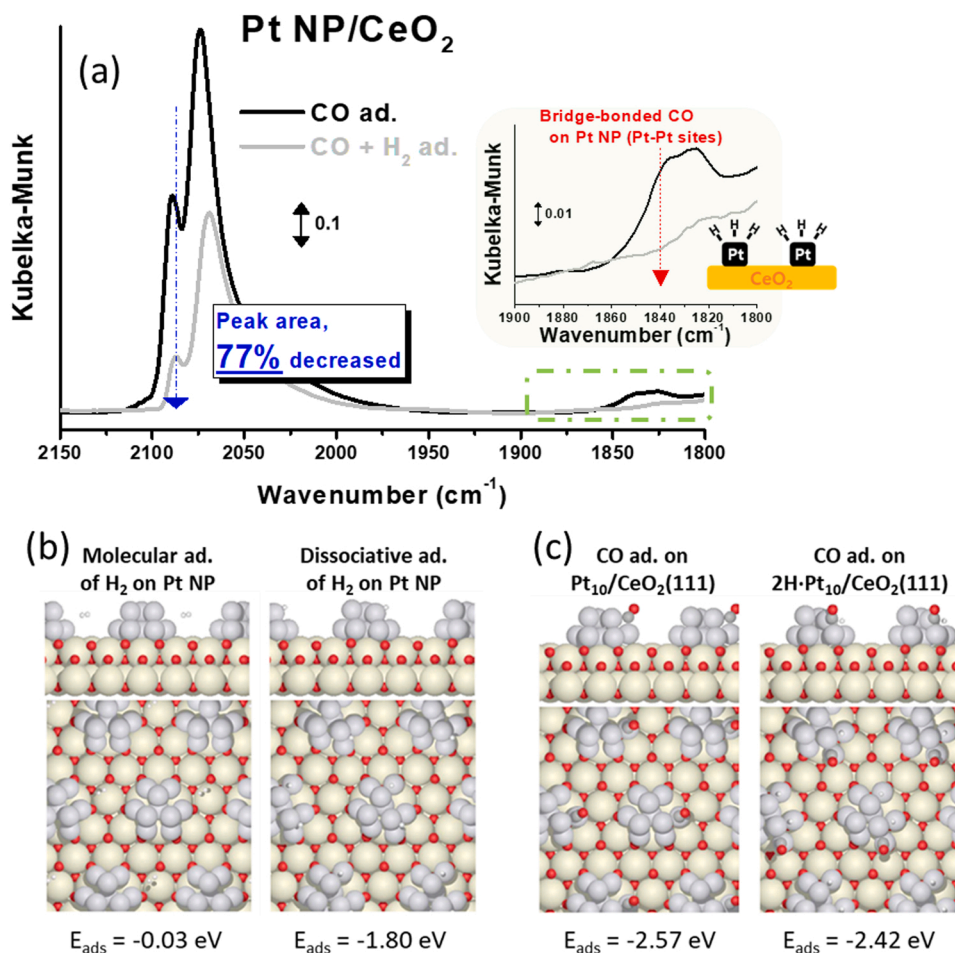


**Fig. 6.** (a) *In-situ* CO-DRIFTS spectra of Pt NP/CeO<sub>2</sub> collected after the pretreatment with H<sub>2</sub> at 400 °C followed by the CO adsorption at 50 °C for 1 hr in the presence or absence of H<sub>2</sub>. The area of the shoulder peak at ~2090 cm<sup>-1</sup> of each spectrum was estimated from the deconvoluted peak (Fig. S18). The inset figure magnifies the spectra in the wavenumber region of 1800–1900 cm<sup>-1</sup>. (b) DFT calculated molecular adsorption and dissociative adsorption energies of H<sub>2</sub> on Pt<sub>10</sub>/CeO<sub>2</sub>(111) are compared. (c) DFT calculated CO adsorption energies on Pt<sub>10</sub>/CeO<sub>2</sub>(111) with and without the adsorbed H are compared. Beige, Red, light grey and dark grey color represent Ce, O, Pt and C atoms, respectively.

Pt NP ( $E_{\text{ads}}$ ,  $-0.03$  vs  $-1.80$  eV). Similar to the 1st H<sub>2</sub> molecule, the 2nd and the 3rd H<sub>2</sub> molecules also favored the dissociative adsorption on Pt NP (Fig. S17 and Table S4), indicating that it occurs readily as long as Pt-Pt contiguous sites are present on the surface. In agreement with the present result, López et al. also reported that the H<sub>2</sub> dissociative activation requires non-negligible activation energy of 1.35 eV on Pt<sub>1</sub>/CeO<sub>2</sub> [71]. Libuda et al. also reported that dissociative activation of H<sub>2</sub> occurs readily on Pt<sub>6</sub> cluster on CeO<sub>2</sub> surface, while it requires high activation barrier of 1.2 eV on Pt single atom [72]. These studies indicate that Pt-Pt sites are necessary for the facile H<sub>2</sub> dissociation.

Fig. 6c shows that the CO adsorption on H-covered Pt NP is unfavorable compared to the CO adsorption on H-free Pt NP ( $E_{\text{ads}}$ ,  $-2.42$  vs  $-2.57$  eV). In addition, when three H<sub>2</sub> molecules were activated on Pt NP, the CO adsorption energy ( $E_{\text{ads}}$ ) increased (or adsorption strength decreased) by up to 0.58 eV (Fig. S17 and Table S4). The size of Pt NP or the CeO<sub>2</sub> facet interacting with Pt NP in our DFT model will differ from the actual catalysts. However, the DFT calculation results in Fig. 6c and S17 demonstrate that H atoms readily activated on the Pt NP surface in the presence of H<sub>2</sub> will interfere with the CO adsorption on Pt. Especially, the area of the peak at ~2090 cm<sup>-1</sup> from CO adsorbed on the Pt NP-CeO<sub>2</sub> interface decreased by 77% when H<sub>2</sub> was added to the feed (the peak area was estimated from the deconvoluted spectra in Fig. S18.) The inhibited CO adsorption on the Pt NP-CeO<sub>2</sub> interface, the active sites of the LT-WGS reaction, by the addition of H<sub>2</sub> could clearly explain the reduced activity of Pt NP/CeO<sub>2</sub> in the LT-WGS reaction as displayed in Fig. 1a.

### 3.4.2. The case of CeO<sub>2</sub>/Pt NP/CeO<sub>2</sub> catalysts

Fig. 7 displays *in-situ* CO-DRIFTS spectra of CeO<sub>2</sub>/Pt NP/CeO<sub>2</sub> 700 R

and 700NC catalysts collected after CO adsorption at 50 °C for 1 h in the presence and absence of H<sub>2</sub>. The area of the peak at ~2090 cm<sup>-1</sup> from CO adsorbed on Pt NP-CeO<sub>2</sub> interface of CeO<sub>2</sub>/Pt NP/CeO<sub>2</sub> 700NC decreased by 21% when H<sub>2</sub> was added to the feed (Fig. 7a). Likewise, the area of the peak at ~2090 cm<sup>-1</sup> from CO adsorbed on Pt NP-CeO<sub>2</sub> interface of CeO<sub>2</sub>/Pt NP/CeO<sub>2</sub> 700 R was not affected by the inclusion of H<sub>2</sub> in the feed (Fig. 7b). These are much less than the case on Pt NP/CeO<sub>2</sub> where the area of the peak at ~2090 cm<sup>-1</sup> decreased by 77% when H<sub>2</sub> was added to the feed (Fig. 6a). Note that the experimental condition employed to collect the *in-situ* DRIFTS spectra is different from the actual reaction condition. For example, we did not include H<sub>2</sub>O in the feed, and the spectra were collected at 50 °C. However, our spectroscopic studies still provide useful information on the inhibitory effect of H<sub>2</sub> on the CO adsorption at the Pt NP-CeO<sub>2</sub> interface.

The area of the peak at ~2090 cm<sup>-1</sup> decreased by 77%, 21% and 0% on Pt NP/CeO<sub>2</sub>, CeO<sub>2</sub>/Pt NP/CeO<sub>2</sub> 700NC and 700 R catalysts, respectively, with the inclusion of H<sub>2</sub> in the feed (from Figs. 6a and 7). Meanwhile, the LT-WGS reaction activity of Pt NP/CeO<sub>2</sub>, CeO<sub>2</sub>/Pt NP/CeO<sub>2</sub> 700NC and 700 R catalysts decreased by 81%, 21% and 13%, respectively, with the inclusion of H<sub>2</sub> in the feed (from Fig. 1). Such correlation between the two variables (the reduction in the area of the ~2090 cm<sup>-1</sup> band and the LT-WGS reaction activity) indicates that the number of accessible CO adsorption sites at the Pt NP-CeO<sub>2</sub> interface would determine the WGS reaction activity. This correlation also indicates that CO-FTIR spectra has the potential to quantify the number of active sites in Pt/CeO<sub>2</sub> catalysts. The activities of CeO<sub>2</sub>/Pt NP/CeO<sub>2</sub> catalysts appear to be more resistant to H<sub>2</sub> since the CO adsorption on its Pt NP-CeO<sub>2</sub> interface is less sensitive to the presence of H<sub>2</sub> in the feed. As demonstrated in DFT calculation results in Fig. 6b, the dissociative

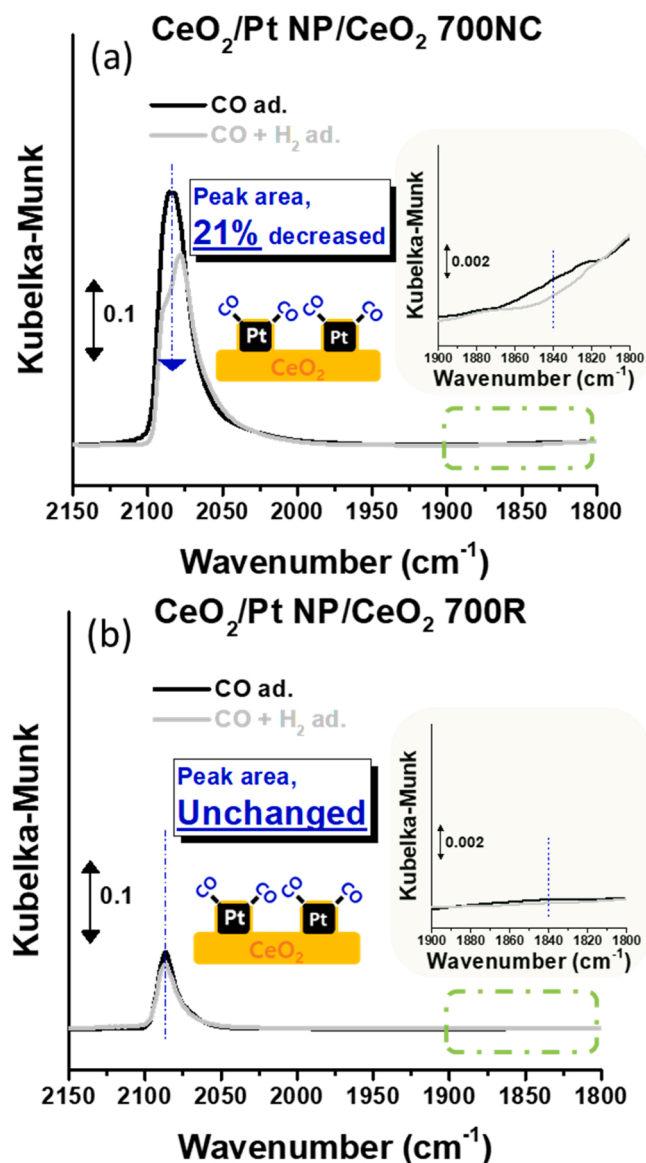


Fig. 7. *In-situ* CO-DRIFTS spectra of  $\text{CeO}_2/\text{Pt NP}/\text{CeO}_2$  700NC (a) and 700R (b) catalysts collected after the pretreatment with  $\text{H}_2$  at  $400^\circ\text{C}$  followed by the CO adsorption at  $50^\circ\text{C}$  for 1 h in the presence or absence of  $\text{H}_2$ . The inset figure in (a) and (b) magnifies the spectra in the wavenumber region of  $1800\text{--}1900\text{ cm}^{-1}$ .

adsorption of  $\text{H}_2$  was favored over the molecular adsorption of  $\text{H}_2$  on Pt NP ( $E_{\text{ads}}$ ,  $-0.03$  vs  $-1.80$  eV). The large adsorption energy of H atom on Pt atom would drive the dissociation of  $\text{H}_2$  on the neighboring Pt sites on Pt NP, [47,73] the presence of which could be identified by the bridge-bonded CO peak at  $1840\text{ cm}^{-1}$  in the CO-DRIFTS spectra. On the CO-DRIFTS spectra of Pt NP/ $\text{CeO}_2$  catalyst collected in the absence of  $\text{H}_2$  (Figs. 2a and 6 a), the presence of the peak at  $1840\text{ cm}^{-1}$  is vividly observed. On the contrary, on the CO-DRIFTS spectra of  $\text{CeO}_2/\text{Pt NP}/\text{CeO}_2$  catalysts collected in the absence of  $\text{H}_2$  (Figs. 2a and 7), the peak at  $1840\text{ cm}^{-1}$  was hardly observed. Hence, only little amount of the neighboring Pt sites would be exposed on  $\text{CeO}_2/\text{Pt NP}/\text{CeO}_2$  catalysts. The  $\text{CeO}_2$  nano-patches formed on Pt NP of  $\text{CeO}_2/\text{Pt NP}/\text{CeO}_2$  catalysts during the  $\text{CeO}_2$  agglomeration would have hindered the exposure of the neighboring Pt sites on Pt NP to suppress the dissociation of  $\text{H}_2$  on Pt NP.

Finally, we could reach the conclusion on how  $\text{H}_2$  affects the LT-WGS reaction activity of Pt/ $\text{CeO}_2$  catalysts. Although Pt NP/ $\text{CeO}_2$  catalyst displayed superior LT-WGS reaction activity than  $\text{CeO}_2/\text{Pt NP}/\text{CeO}_2$  700NC catalyst under the feed without  $\text{H}_2$ ,  $\text{CeO}_2/\text{Pt NP}/\text{CeO}_2$  700NC

catalyst displayed the higher LT-WGS reaction activity when  $\text{H}_2$  was added to the feed. While the Pt NP- $\text{CeO}_2$  interface catalyzes the LT-WGS reaction,  $\text{H}_2$  activated on the Pt-Pt sites of Pt NP would interfere with the CO adsorption at the active sites. As a result, the addition of  $\text{H}_2$  to the feed significantly decreased the activity of Pt NP/ $\text{CeO}_2$  catalyst. On the other hand, on  $\text{CeO}_2/\text{Pt NP}/\text{CeO}_2$  catalysts,  $\text{CeO}_2$  nano-patches partially covering Pt NP prohibits the exposure of the neighboring Pt sites, while facilitating the formation of the active Pt NP- $\text{CeO}_2$  interface. As a result, the LT-WGS reaction could proceed on  $\text{CeO}_2/\text{Pt NP}/\text{CeO}_2$  catalysts with only the minute disturbance from the presence of  $\text{H}_2$  in the feed. In other words, the  $\text{CeO}_2$  nano-patches on Pt NP in  $\text{CeO}_2/\text{Pt NP}/\text{CeO}_2$  catalysts decreases the H coverage at the Pt NP- $\text{CeO}_2$  interface, resulting in alleviating the inhibitory effect of  $\text{H}_2$  in the LT-WGS reaction.

Engineering the metal-support interface has gained much attention as a means to improve catalytic activity [59,74,75]. In this study, Pt/ $\text{CeO}_2$  catalysts exposing dominantly the metal-support interface were successfully prepared via the simple reductive treatment. In many cases, the interface between PGM NP and metal-oxide support possesses the high catalytic activity [59,74–78]. For this reason, many interesting strategies have been developed to maximize the active interfacial area. For example, Gutiérrez et al. synthesized inverse iron oxide/metal catalysts by using the galvanic replacement reaction to increase the concentration of oxide species adjoining metal domains [77]. In addition, Zanchet and Dumesic et al. selectively deposited Fe onto Pt NP by using the controlled surface reaction to form the intimate contact between Pt and Fe [78]. However, little attention has been devoted to understanding how the catalytic activity of the interface would be affected by the PGM NP forming the interface. In this study, the LT-WGS reaction activity of Pt/ $\text{CeO}_2$  catalyst was enhanced 3.5 times by forming  $\text{CeO}_2$  nano-patches on Pt NP surface to suppress the exposure of paired Pt sites. Such results highlight that constructing a proper catalysts' structure could be an effective strategy to optimize the catalytic activity of the interface under practical conditions.

#### 4. Conclusion

The influence of the presence of  $\text{H}_2$  on the activity of Pt/ $\text{CeO}_2$  catalysts in the LT-WGS reaction was investigated in this contribution. *In-situ* CO-DRIFTS spectra were used to characterize the catalytic active sites and to unravel the effect of  $\text{H}_2$  on the catalytic activity.  $\text{H}_2$  greatly decreased the WGS reaction activity of Pt NP/ $\text{CeO}_2$  catalyst while the activity of  $\text{CeO}_2/\text{Pt NP}/\text{CeO}_2$  catalysts were mostly preserved. It was found that the dissociative adsorption of  $\text{H}_2$  on the neighboring Pt sites on Pt NP interfered with the adsorption of CO on the Pt NP- $\text{CeO}_2$  interface, the catalytic active sites. On the other hand, the thin  $\text{CeO}_2$  nano-patches on Pt NP suppressed the exposure of the neighboring Pt sites, while facilitating the formation of Pt NP- $\text{CeO}_2$  interface. For this reason, the LT-WGS reaction activities of  $\text{CeO}_2/\text{Pt NP}/\text{CeO}_2$  catalysts were less affected by the presence of  $\text{H}_2$  in the feed. Importantly, the LT-WGS reaction activity of Pt/ $\text{CeO}_2$  catalyst under the feed gas containing excess  $\text{H}_2$  was enhanced more than three times by forming thin  $\text{CeO}_2$  nano-patches on Pt NP. This study highlights that the catalytic activity under the practical operating condition could be improved to the great extent by constructing an appropriate catalysts' structure.

#### CRedit authorship contribution statement

**Jaeha Lee:** Conceptualization, Investigation, Writing – original draft preparation, Writing – review & editing, **Dongjae Shin:** Investigation, Writing – review & editing, **Eunwon Lee:** Investigation, Writing – review & editing, **Chengbin Li:** Investigation, Writing – review & editing, **Ji Man Kim:** Conceptualization, Writing – review & editing, **Jeong Woo Han:** Conceptualization, Writing – review & editing, **Do Heui Kim:** Supervision, Funding acquisition, Conceptualization, Writing – review & editing.

## Declaration of Competing Interest

The authors declare that they have no known competing financial interests or personal relationships that could have appeared to influence the work reported in this paper.

## Acknowledgements

This work was supported by a National Research Foundation of Korea (NRF) grant funded by the Korean government (MSIP) (NRF-2016R1A5A1009592). The Institute of Engineering Research at Seoul National University partially provided the research facilities for this work.

## Supporting information

Additional related WGS reactivity, CO and O<sub>2</sub> chemisorption, CO-DRIFTS spectra, XPS spectra, HAADF-STEM images and DFT calculation results.

## Appendix A. Supporting information

Supplementary data associated with this article can be found in the online version at doi:10.1016/j.apcatb.2021.121038.

## References

- [1] C. Ratnasamy, J.P. Wagner, Water gas shift catalysis, *Catal. Rev. Sci. Eng.* 51 (2009) 325–440.
- [2] T.L. LeValley, A.R. Richard, M. Fan, The progress in water gas shift and steam reforming hydrogen production technologies—a review, *Int. J. Hydrog. Energy* 39 (2014) 16983–17000.
- [3] Z.-S. Zhang, Q. Fu, K. Xu, W.-W. Wang, X.-P. Fu, X.-S. Zheng, K. Wu, C. Ma, R. Si, C.-J. Jia, Intrinsically active surface in a Pt/γ-Mo<sub>2</sub>N catalyst for the water–gas shift reaction: molybdenum nitride or molybdenum oxide? *J. Am. Chem. Soc.* 142 (2020) 13362–13371.
- [4] J.H. Carter, X. Liu, Q. He, S. Althahban, E. Nowicka, S.J. Freakley, L. Niu, D. J. Morgan, Y. Li, J. Niemantsverdriet, Activation and deactivation of gold/ceria–zirconia in the low-temperature water–gas shift reaction, *Angew. Chem.* 56 (2017) 16037–16041.
- [5] N. Liu, M. Xu, Y. Yang, S. Zhang, J. Zhang, W. Wang, L. Zheng, S. Hong, M. Wei, Au<sup>δ−</sup>–O<sub>v</sub>–Ti<sup>3+</sup> interfacial site: catalytic active center toward low-temperature water gas shift reaction, *ACS Catal.* 9 (2019) 2707–2717.
- [6] Y. Chen, J. Lin, L. Li, B. Qiao, J. Liu, Y. Su, X. Wang, Identifying size effects of Pt as single atoms and nanoparticles supported on FeO<sub>x</sub> for the water–gas shift reaction, *ACS Catal.* 8 (2018) 859–868.
- [7] D. Carta, T. Montini, M.F. Casula, M. Monai, S. Bullita, P. Fornasiero, A. Corrias, The water gas shift reaction over Pt–CeO<sub>2</sub> nanoparticles confined within mesoporous SBA-16, *J. Mater. Chem. A* 5 (2017) 20024–20034.
- [8] Y.-L. Lee, A. Mnoyan, H.-S. Na, S.-Y. Ahn, K.-J. Kim, J.-O. Shim, K. Lee, H.-S. Roh, Comparison of the effects of the catalyst preparation method and CeO<sub>2</sub> morphology on the catalytic activity of Pt/CeO<sub>2</sub> catalysts for the water–gas shift reaction, *Catal. Sci. Technol.* 10 (2020) 6299–6308.
- [9] J.H. Carter, G.J. Hutchings, Recent advances in the gold-catalysed low-temperature water–gas shift reaction, *Catalysts* 8 (2018) 627.
- [10] Y.M. Park, M. Son, M.-J. Park, J.W. Bae, Effects of Pt precursors on Pt/CeO<sub>2</sub> to water–gas shift (WGS) reaction activity with Langmuir–Hinshelwood model-based kinetics, *Int. J. Hydrog. Energy* 45 (2020) 26953–26966.
- [11] J. Lee, C. Li, S. Kang, J. Park, J.M. Kim, D.H. Kim, Pt nanoparticles encapsulated in CeO<sub>2</sub> over-layers synthesized by controlled reductive treatment to suppress CH<sub>4</sub> formation in high-temperature water–gas shift reaction, *J. Catal.* 395 (2021) 246–257.
- [12] Y. Li, M. Kottwitz, J.L. Vincent, M.J. Enright, Z. Liu, L. Zhang, J. Huang, S. D. Senanayake, W.-C.D. Yang, P.A. Crozier, Dynamic structure of active sites in ceria-supported Pt catalysts for the water gas shift reaction, *Nat. Commun.* 12 (2021) 1–9.
- [13] K. Yuan, Y. Guo, Q.-L. Lin, L. Huang, J.-T. Ren, H.-C. Liu, C.-H. Yan, Y.-W. Zhang, Size effect-tuned water gas shift reaction activity and pathway on ceria supported platinum catalysts, *J. Catal.* 394 (2021) 121–130.
- [14] M. Yang, J. Liu, S. Lee, B. Zugic, J. Huang, L.F. Allard, M. Flytzani-Stephanopoulos, A common single-site Pt(II)–O(OH)<sub>x</sub>-species stabilized by sodium on “active” and “inert” supports catalyzes the water–gas shift reaction, *J. Am. Chem. Soc.* 137 (2015) 3470–3473.
- [15] J. Vecchiotti, A. Bonivardi, W. Xu, D. Stacchiola, J.J. Delgado, M. Calatayud, S.N. E. Collins, Understanding the role of oxygen vacancies in the water gas shift reaction on ceria-supported platinum catalysts, *ACS Catal.* 4 (2014) 2088–2096.
- [16] C. Kalamaras, D. Dionysiou, A. Efstathiou, Mechanistic studies of the water–gas shift reaction over Pt/Ce<sub>x</sub>Zr<sub>1-x</sub>O<sub>2</sub> catalysts: the effect of Pt particle size and Zr dopant, *ACS Catal.* 2 (2012) 2729–2742.
- [17] A. Bruix, J.A. Rodriguez, P.J. Ramirez, S.D. Senanayake, J. Evans, J.B. Park, D. Stacchiola, P. Liu, J. Hrbek, F. Illas, A new type of strong metal–support interaction and the production of H<sub>2</sub> through the transformation of water on Pt/CeO<sub>2</sub>(111) and Pt/CeO<sub>x</sub>/TiO<sub>2</sub>(110) catalysts, *J. Am. Chem. Soc.* 134 (2012) 8968–8974.
- [18] S. Aranifard, S.C. Ammal, A. Heyden, On the importance of metal–oxide interface sites for the water–gas shift reaction over Pt/CeO<sub>2</sub> catalysts, *J. Catal.* 309 (2014) 314–324.
- [19] X.-P. Fu, L.-W. Guo, W.-W. Wang, C. Ma, C.-J. Jia, K. Wu, R. Si, L.-D. Sun, C.-H. Yan, Direct identification of active surface species for the water–gas shift reaction on a gold–ceria catalyst, *J. Am. Chem. Soc.* 141 (2019) 4613–4623.
- [20] N.C. Nelson, J. Szanyi, Heterolytic hydrogen activation: understanding support effects in water–gas shift, hydrodeoxygenation, and CO oxidation catalysis, *ACS Catal.* 10 (2020) 5663–5671.
- [21] N.C. Nelson, M.-T. Nguyen, V.-A. Glezakou, R. Rousseau, J. Szanyi, Carboxyl intermediate formation via an in situ-generated metastable active site during water–gas shift catalysis, *Nat. Catal.* 2 (2019) 916–924.
- [22] C.M. Kalamaras, S. Americanou, A.M. Efstathiou, “Redox” vs “associative formate with–OH group regeneration” WGS reaction mechanism on Pt/CeO<sub>2</sub>: effect of platinum particle size, *J. Catal.* 279 (2011) 287–300.
- [23] S. Yao, X. Zhang, W. Zhou, R. Gao, W. Xu, Y. Ye, L. Lin, X. Wen, P. Liu, B. Chen, Atomic-layered Au clusters on α-MoC as catalysts for the low-temperature water–gas shift reaction, *Science* 357 (2017) 389–393.
- [24] O. Thinnon, K. Rachedi, F. Diehl, P. Avenier, Y. Schuurman, Kinetics and mechanism of the water–gas shift reaction over platinum supported catalysts, *Top. Catal.* 52 (2009) 1940–1945.
- [25] G. Germani, Y. Schuurman, Water–gas shift reaction kinetics over μ-structured Pt/CeO<sub>2</sub>/Al<sub>2</sub>O<sub>3</sub> catalysts, *AIChE J.* 52 (2006) 1806–1813.
- [26] J. Lee, Y. Ryou, X. Chan, T.J. Kim, D.H. Kim, How Pt interacts with CeO<sub>2</sub> under the reducing and oxidizing environments at elevated temperature: the origin of improved thermal stability of Pt/CeO<sub>2</sub> compared to CeO<sub>2</sub>, *J. Phys. Chem. C* 120 (2016) 25870–25879.
- [27] X. Ye, H. Wang, Y. Lin, X. Liu, L. Cao, J. Gu, J. Lu, Insight of the stability and activity of platinum single atoms on ceria, *Nano Res.* 12 (2019) 1401–1409.
- [28] J. Resasco, L. DeRita, S. Dai, J.P. Chada, M. Xu, X. Yan, J. Finzel, S. Hanukovich, A. S. Hoffman, G.W. Graham, Uniformity is key in defining structure–function relationships for atomically dispersed metal catalysts: the case of Pt/CeO<sub>2</sub>, *J. Am. Chem. Soc.* 142 (2019) 169–184.
- [29] D. Kunwar, S. Zhou, A. DeLaRiva, E.J. Peterson, H. Xiong, X.I. Pereira-Hernández, S.C. Purdy, R. ter Veen, H.H. Brongersma, J.T. Miller, Stabilizing high metal loadings of thermally stable platinum single atoms on an industrial catalyst support, *ACS Catal.* 9 (2019) 3978–3990.
- [30] X.I. Pereira-Hernández, A. DeLaRiva, V. Muravev, D. Kunwar, H. Xiong, B. Sudduth, M. Engelhard, L. Kovarik, E.J. Hensen, Y. Wang, Tuning Pt–CeO<sub>2</sub> interactions by high-temperature vapor-phase synthesis for improved reducibility of lattice oxygen, *Nat. Commun.* 10 (2019) 1358.
- [31] A. Borodziński, M. Bonarowska, Relation between crystallite size and dispersion on supported metal catalysts, *Langmuir* 13 (1997) 5613–5620.
- [32] T. Tanabe, Y. Nagai, T. Hirabayashi, N. Takagi, K. Dohmae, N. Takahashi, Si Matsumoto, H. Shinjoh, J.N. Kondo, J.C. Schouten, Low temperature CO pulse adsorption for the determination of Pt particle size in a Pt/ceria-based oxide catalyst, *Appl. Catal. A: Gen.* 370 (2009) 108–113.
- [33] J. Freil, Chemisorption on supported platinum: II. Stoichiometry for hydrogen, oxygen and carbon monoxide, *J. Catal.* 25 (1972) 149–160.
- [34] L.F. Liotta, A. Longo, A. Macaluso, A. Martorana, G. Pantaleo, A.M. Venezia, G. Deganello, Influence of the SMSI effect on the catalytic activity of a Pt(1%)/CeO<sub>2</sub>/ZrO<sub>2</sub> catalyst: SAXS, XRD, XPS and TPR investigations, *Appl. Catal. B: Environ.* 48 (2004).
- [35] G. Kresse, J. Furthmüller, Efficient iterative schemes for ab initio total-energy calculations using a plane-wave basis set, *Phys. Rev. B* 54 (1996) 11169–11186.
- [36] S. Dudarev, G. Botton, S. Savrasov, C. Humphreys, A. Sutton, Electron-energy-loss spectra and the structural stability of nickel oxide: an LSDA+ U study, *Phys. Rev. B* 57 (1998) 1505–1509.
- [37] K.-J. Noh, K. Kim, H.J. Kim, D. Shin, J.W. Han, Improved CO oxidation via surface stabilization of ceria nanoparticles induced by rare-earth metal dopants, *ACS Appl. Nano Mater.* 2 (2019) 6473–6481.
- [38] S. Aranifard, S.C. Ammal, A. Heyden, Nature of Pt<sub>n</sub>/CeO<sub>2</sub>(111) surface under water–gas shift reaction conditions: a constrained ab initio thermodynamics study, *J. Phys. Chem. C* 116 (2012) 9029–9042.
- [39] Pt<sub>2</sub>O. Crystal Structure: Datasheet from “PAULING FILE Multinaries Edition – 2012” in SpringerMaterials ((https://materials.springer.com/isp/crystallographic/docs/sd.0260837)), Springer-Verlag Berlin Heidelberg & Material Phases Data System (MPDS), Switzerland & National Institute for Materials Science (NIMS), Japan.
- [40] T. Jacob, Theoretical investigations on the potential-induced formation of Pt-oxide surfaces, *J. Electroanal. Chem.* 607 (2007) 158–166.
- [41] L. Yang, Y.L. Zhao, K. Li, Z.C. Chen, P. Zhang, W.Q. Shi, Adsorption of CH<sub>3</sub>I on Ag(111) and Ag<sub>2</sub>O(111) surface: a density functional theory study, *Chem. Phys.* 513 (2018) 35–40.
- [42] A.K. Mishra, A. Roldan, N.H. de Leeuw, A density functional theory study of the adsorption behaviour of CO<sub>2</sub> on Cu<sub>2</sub>O surfaces, *J. Chem. Phys.* 145 (2016), 044709.

- [43] N.E. Singh-Miller, N. Marzari, Surface energies, work functions, and surface relaxations of low-index metallic surfaces from first principles, *Phys. Rev. B* 80 (2009), 235407.
- [44] M.G. Castaño, T. Reina, S. Ivanova, M. Centeno, J. Odriozola, Pt vs. Au in water–gas shift reaction, *J. Catal.* 314 (2014) 1–9.
- [45] C.A. Callaghan, Kinetics and catalysis of the water-gas-shift reaction: a microkinetic and graph theoretic approach, *Worcester. Polytech. Inst.* (2006).
- [46] L. Liu, A. Corma, Identification of the active sites in supported subnanometric metal catalysts, *Nat. Catal.* 4 (2021) 1–4.
- [47] L. Liu, D.M. Meira, R. Arenal, P. Concepcion, A.V. Puga, A. Corma, Determination of the evolution of heterogeneous single metal atoms and nanoclusters under reaction conditions: which are the working catalytic sites? *ACS Catal.* 9 (2019) 10626–10639.
- [48] M. Macino, A.J. Barnes, S.M. Althabhan, R. Qu, E.K. Gibson, D.J. Morgan, S. J. Freakley, N. Dimitratos, C.J. Kiely, X. Gao, Tuning of catalytic sites in Pt/TiO<sub>2</sub> catalysts for the chemoselective hydrogenation of 3-nitrostyrene, *Nat. Catal.* 2 (2019) 873–881.
- [49] T. Kropp, Z. Lu, Z. Li, Y.-H.C. Chin, M. Mavrikakis, Anionic single-atom catalysts for CO oxidation: Support-independent activity at low temperatures, *ACS Catal.* 9 (2019) 1595–1604.
- [50] M.J. Kale, P. Christopher, Utilizing quantitative in situ FTIR spectroscopy to identify well-coordinated Pt atoms as the active site for CO oxidation on Al<sub>2</sub>O<sub>3</sub>-supported Pt catalysts, *ACS Catal.* 6 (2016) 5599–5609.
- [51] B. Qiao, A. Wang, X. Yang, L.F. Allard, Z. Jiang, Y. Cui, J. Liu, J. Li, T. Zhang, Single-atom catalysis of CO oxidation using Pt<sub>1</sub>/FeO<sub>x</sub>, *Nat. Chem.* 3 (2011) 634–641.
- [52] M.J. Lundwall, S.M. McClure, D.W. Goodman, Probing terrace and step sites on Pt nanoparticles using CO and ethylene, *J. Phys. Chem. C* 114 (2010) 7904–7912.
- [53] R.K. Brandt, M. Hughes, L. Bourget, K. Truszkowska, R.G. Greenler, The interpretation of CO adsorbed on Pt/SiO<sub>2</sub> of two different particle-size distributions, *Surf. Sci.* 286 (1993) 15–25.
- [54] J. Yoshinobu, N. Tsukahara, F. Yasui, K. Mukai, Y. Yamashita, Lateral displacement by transient mobility in chemisorption of CO on Pt (1997), *Phys. Rev. Lett.* 90 (2003), 248301.
- [55] P. Bazin, O. Saur, J. Lavalley, M. Daturi, G. Blanchard, FT-IR study of CO adsorption on Pt/CeO<sub>2</sub>: characterisation and structural rearrangement of small Pt particles, *Phys. Chem. Chem. Phys.* 7 (2005) 187–194.
- [56] M. Happel, J. Mysliveček, V. Johánek, F. Dvořák, O. Stetsovych, Y. Lykhach, V. Matolín, J. Libuda, Adsorption sites, metal-support interactions, and oxygen spillover identified by vibrational spectroscopy of adsorbed CO: a model study on Pt/ceria catalysts, *J. Catal.* 289 (2012) 118–126.
- [57] H.A. Aleksandrov, K.M. Neyman, K.I. Hadjiivanov, G.N. Vayssilov, Can the state of platinum species be unambiguously determined by the stretching frequency of an adsorbed CO probe molecule? *Phys. Chem. Chem. Phys.* 18 (2016) 22108–22121.
- [58] S. Tauster, S. Fung, R. Garten, Strong metal-support interactions. group 8 noble metals supported on titanium dioxide, *J. Am. Chem. Soc.* 100 (1978) 170–175.
- [59] I. Ro, J. Resasco, P. Christopher, Approaches for understanding and controlling interfacial effects in oxide-supported metal catalysts, *ACS Catal.* 8 (2018) 7368–7387.
- [60] S. Zhang, P.N. Plessow, J.J. Willis, S. Dai, M. Xu, G.W. Graham, M. Cargnello, F. Abild-Pedersen, X. Pan, Dynamical observation and detailed description of catalysts under strong metal–support interaction, *Nano Lett.* 16 (2016) 4528–4534.
- [61] Q. Fu, H. Saltsburg, M. Flytzani-Stephanopoulos, Active nonmetallic Au and Pt species on ceria-based water-gas shift catalysts, *Science* 301 (2003) 935–938.
- [62] Y. Zhai, D. Pierre, R. Si, W. Deng, P. Ferrin, A.U. Nilekar, G. Peng, J.A. Herron, D. C. Bell, H. Saltsburg, M. Mavrikakis, M. Flytzani-Stephanopoulos, Alkali-stabilized Pt-OH<sub>x</sub> species catalyze low-temperature water-gas shift reactions, *Science* 329 (2010) 1633–1636.
- [63] S. Chen, C. Pei, J. Gong, Insights into interface engineering in steam reforming reactions for hydrogen production, *Energy Environ. Sci.* 12 (2019) 3473–3495.
- [64] A.M. Efstathiou, Elucidation of mechanistic and kinetic aspects of water–gas shift reaction on supported Pt and Au catalysts via transient isotopic techniques, *Catalysis* 28 (2016) 175–236.
- [65] J. Rodriguez, S. Ma, P. Liu, J. Hrbek, J. Evans, M. Perez, Activity of CeO<sub>x</sub> and TiO<sub>x</sub> nanoparticles grown on Au (111) in the water-gas shift reaction, *Science* 318 (2007) 1757–1760.
- [66] J.B. Park, J. Graciani, J. Evans, D. Stacchiola, S.D. Senanayake, L. Barrio, P. Liu, J. F. Sanz, J. Hrbek, J.A. Rodriguez, Gold, copper, and platinum nanoparticles dispersed on CeO<sub>x</sub>/TiO<sub>2</sub> (110) surfaces: high water-gas shift activity and the nature of the mixed-metal oxide at the nanometer level, *J. Am. Chem. Soc.* 132 (2010) 356–363.
- [67] P. Panagiotopoulou, D.I. Kondarides, A comparative study of the water-gas shift activity of Pt catalysts supported on single (MO<sub>x</sub>) and composite (MO<sub>x</sub>/Al<sub>2</sub>O<sub>3</sub>, MO<sub>x</sub>/TiO<sub>2</sub>) metal oxide carriers, *Catal. Today* 127 (2007) 319–329.
- [68] X. Zhu, M. Shen, L.L. Lobban, R.G. Mallinson, Structural effects of Na promotion for high water gas shift activity on Pt–Na/TiO<sub>2</sub>, *J. Catal.* 278 (2011) 123–132.
- [69] D. Pierre, W. Deng, M. Flytzani-Stephanopoulos, The importance of strongly bound Pt–CeO<sub>x</sub> species for the water-gas shift reaction: catalyst activity and stability evaluation, *Top. Catal.* 46 (2007) 363–373.
- [70] S. Zhang, J.-j. Shan, Y. Zhu, A.I. Frenkel, A. Patlolla, W. Huang, S.J. Yoon, L. Wang, H. Yoshida, S. Takeda, WGS catalysis and in situ studies of CoO<sub>1-x</sub>, PtCo<sub>n</sub>/Co<sub>3</sub>O<sub>4</sub>, and Pt<sub>m</sub>Co<sub>m</sub>/CoO<sub>1-x</sub> nanorod catalysts, *J. Am. Chem. Soc.* 135 (2013) 8283–8293.
- [71] N. Daelman, M. Capdevila-Cortada, N. López, Dynamic charge and oxidation state of Pt/CeO<sub>2</sub> single-atom catalysts, *Nat. Mater.* 18 (2019) 1215–1221.
- [72] Y. Lykhach, A. Figueroba, M.F. Camellone, A. Neitzel, T. Skála, F.R. Negreiros, M. Vorokhta, N. Tsud, K.C. Prince, S. Fabris, Reactivity of atomically dispersed Pt<sup>2+</sup> species towards H<sub>2</sub>: model Pt–CeO<sub>2</sub> fuel cell catalyst, *Phys. Chem. Chem. Phys.* 18 (2016) 7672–7679.
- [73] N. Acerbi, S. Tsang, G. Jones, S. Golunski, P. Collier, Rationalization of interactions in precious metal/ceria catalysts using the d-band center model, *Angew. Chem. Int. Ed.* 52 (2013) 7737–7741.
- [74] T.W. van Deelen, C.H. Mejía, K.P. de Jong, Control of metal-support interactions in heterogeneous catalysts to enhance activity and selectivity, *Nat. Catal.* 2 (2019) 1–16.
- [75] A.K. Datye, M. Votsmeier, Opportunities and challenges in the development of advanced materials for emission control catalysts, *Nat. Mater.* 20 (2020) 1–11.
- [76] M. Cargnello, V.V. Doan-Nguyen, T.R. Gordon, R.E. Diaz, E.A. Stach, R.J. Gorte, P. Fornasiero, C.B. Murray, Control of metal nanocrystal size reveals metal-support interface role for ceria catalysts, *Science* 341 (2013) 771–773.
- [77] Y. Zhu, X. Zhang, K. Koh, L. Kovarik, J.L. Fulton, K.M. Rosso, O.Y. Gutiérrez, Inverse iron oxide/metal catalysts from galvanic replacement, *Nat. Commun.* 11 (2020) 1–7.
- [78] I.B. Aragao, I. Ro, Y. Liu, M. Ball, G.W. Huber, D. Zanchet, J.A. Dumesic, Catalysts synthesized by selective deposition of Fe onto Pt for the water-gas shift reaction, *Appl. Catal. B: Environ.* 222 (2018) 182–190.